Distinguishing between Hodographs of Severe Hail and Tornadoes

Cameron J. Nixon,[1] John T. Allen,[1]

[1] *Department of Earth and Atmospheric Sciences, Central Michigan University, Mt. Pleasant, Michigan, USA*

Corresponding author: Brooks Hall 301, Central Michigan University, Mt. Pleasant, MI, 48858, USA. Email: cameron.nixon@cmich.edu

Early Online Release: This preliminary version has been accepted for publication in *Weather and Forecasting* cited, and has been assigned DOI 10.1175/WAF-D-21-0136.1.The final typeset copyedited article will replace the EOR at the above DOI when it is published.

ABSTRACT: Hodographs are valuable sources of pattern recognition in severe convective storm forecasting. Certain shapes are known to discriminate between single cell, multicell, and supercell storm organization. Various derived quantities such as storm-relative helicity (SRH) have been found to predict tornado potential and intensity. Over the years, collective research has established a conceptual model for tornadic hodographs (large and "looping", with high SRH). However, considerably less attention has been given to constructing a similar conceptual model for hodographs of severe hail. This study explores how hodograph shape may differentiate between the environments of severe hail and tornadoes. While supercells are routinely assumed to carry the potential to produce all hazards, this is not always the case, and we explore why. The Storm Prediction Center (SPC) storm mode dataset is used to assess the environments of 8,958 tornadoes and 7,256 severe hail reports, produced by right- and left-moving supercells. Composite hodographs and indices to quantify wind shear are assessed for each hazard, and clear differences are found between the kinematic environments of hail-producing and tornadic supercells. The sensitivity of the hodograph to common thermodynamic variables was also examined, with buoyancy and moisture found to influence the shape associated with the hazards. The results suggest that differentiating between tornadic and hail-producing storms may be possible using properties of the hodograph alone. While anticipating hail size does not appear possible using only the hodograph, anticipating tornado intensity appears readily so. When coupled with buoyancy profiles, the hodograph may assist in differentiating between both hail size and tornado intensity.

Accepted for publication in *Weather and Forecasting.* DOI 10.1175/WAF-D-21-0136.1.

1. Introduction

a. Motivation

The United States faces a variety of severe convective storm hazards that result in the loss of life and property. To communicate forecasts of these hazards, the Storm Prediction Center issues daily convective outlooks that convey the potential for severe hail, severe convective wind gusts, and tornadoes (Hitchens and Brooks 2012). In these outlooks, the potential for supercell storms is frequently addressed. In the cases of both tornadoes and hail of at least 51 mm (2 in) in diameter, supercell storms account for the vast majority of these events (Smith et al. 2012; Blair et al. 2017). When supercells are forecast or ongoing, it is common practice to release an outlook for an area for at least a low threat of all hazards. However, not all supercells are capable of producing both tornadoes and severe hail. Consequently, research into potentially distinguishing between the environmental controls on these supercell hazards is warranted.

Out of tornadoes, large hail, and damaging wind, tornadoes are responsible for the most deaths of the three. However, only a small percentage of tornadoes are deadly (Galway 1975), with EF4–EF5 tornadoes accounting for 67.5% of fatalities despite making up only 2.1% of all tornadoes (Ashley 2007). Severe hail is the most expensive hazard in the United States, responsible for around $10 billion USD in insured losses annually, and with individual events commonly reaching over $1 billion in metropolitan areas (Gunturi and Tippett 2017). Although National Weather Service Weather Forecast Offices (NWS WFOs) issue Severe Thunderstorm Warnings for all instances of reported or suspected severe hail (≥1.0 in), significant-severe hail (≥2.0 in) may carry particularly more damaging safety/economic impacts than smaller hail (Johnson and Sugden 2014; Blair et al. 2017). Annual maximum hail size is highest (over 2.5 in) on average over the southern and central Plains, especially from northern Texas into southern Nebraska (Allen and Tippett 2015; Allen et al. 2017).

b. Background

Past literature has linked specific hodograph shapes to certain hazards and their intensities. Long, straight hodographs have long been associated with splitting supercells, while clockwise curvature of the shear vector with height, especially in the low levels, favors the cyclonic, right-moving supercell (Weisman and Klemp 1986). Particularly strong curvature and "sickle-shaped"

Accepted for publication in *Weather and Forecasting.* DOI 10.1175/WAF-D-21-0136.1.

hodographs (where a layer of strong low-level shear sits beneath an abrupt clockwise turning of the shear vector with height) have become accepted as favorable for significant (EF2 and stronger) tornadoes (Thompson and Edwards 2000), especially those that feature strong shear near the surface (Coffer et al. 2020). More recently, straight hodographs have also been attributed to enhanced hail potential (Johnson and Sugden 2014; Dennis and Kumjian 2017; Kumjian and Lombardo 2020; Kumjian et al. 2021). Extensive work has been done on differentiating between the hodographs of tornadic and non-tornadic supercells (Markowski et al. 2003; Parker 2014; Coffer and Parker 2017; Coniglio and Parker 2020), as well as between the hodographs of weak and significant tornadoes (Esterheld and Giuliano 2008; Nowotarski and Jones 2018; Coffer et al. 2019, 2020). However, little work has been done to directly assess whether or not there are differences between the hodographs of severe hail and tornado-producing supercells, or to assess changes in hodograph characteristics with increasing hazard severity (tornado rating and hail size).

Variables that approximate some general properties of hodograph structure have been regularly used in forecasting (Thompson et al. 2003, 2007, 2012). Storm-relative helicity (SRH) is widely used to forecast supercells and tornadoes, and reflects both the strength of the storm-relative winds and the available streamwise vorticity in the low levels given a particular storm motion (Davies-Jones 1990). SRH in the lowest few kilometers has found use in forecasting supercell storms; as a result, this variable is used independently and employed in the supercell composite parameter (SCP; Thompson et al. 2002, 2004). SRH in the lowest kilometer has similarly shown skill in predicting significant tornadoes, and is used in the significant tornado parameter (STP; Thompson et al. 2002, 2004), with recent work finding that layers closer to the surface show greater skill (Coffer et al. 2019). Bulk wind differences (BWD) also appear in composite parameters (e.g. SCP and STP), and are known to be useful in anticipating storm severity and organization (Brooks et al. 2003; Taszarek et al. 2020). The significant hail parameter (SHIP, `https://www.spc.noaa.gov/exper/mesoanalysis/help/help_sigh.html`) employs 0–6-km BWD (though no published evaluation of its performance is available), while the large hail parameter uses BWD from the surface to the equilibrium level (Johnson and Sugden 2014). Both ground-relative and storm-relative wind magnitude are also used in this parameter, but rarely elsewhere. Storm-relative winds in particular have been found to influence the width and strength of supercell updrafts (Peters et al. 2019, 2020).

Accepted for publication in *Weather and Forecasting.* DOI 10.1175/WAF-D-21-0136.1.

Thermodynamics play a crucial role, in tandem with kinematics, in modulating severe convective storms and their potential hazards. For instance, past research has noted that severe storms can exist across a spectrum of convective available potential energy (CAPE) and wind shear, such that more of one can compensate for less of the other (Johns et al. 1993; Brooks et al. 2003). These studies suggest that strong and violent tornadoes may need less shear for higher CAPE, or less CAPE for higher shear. Thus, while hodograph differences may exist between hazards and their intensities, the role of thermodynamics must not be ignored. To address this, the present study contains an assessment of how the hodograph shape associated with each hazard depends on the accompanying thermodynamic environment. However, the primary goal of this study is to explore the relationship between hazards, their magnitudes, and their associated environmental wind shear profile. Relative differences will be assessed under the presupposition that the wind profile plays a crucial role in supercell organization and structure, which in turn can regulate the production of hazards. Though we will offer insight into the performance of certain wind shear indices to provide context for our analysis, rather than a parameter-based approach, we aim instead to provide a conceptual analysis of what severe hazards should be anticipated with a given hodograph shape.

2. Data and methods

a. Case selection

This study obtained its samples from the hazard–storm mode dataset developed by the Storm Prediction Center (Smith et al. 2012; Thompson et al. 2012). This dataset contains storm reports categorized by hazard, magnitude, storm mode, and various other descriptors, spanning the years 2003–2017. Cases were considered for this study if they occurred during the period from 2005 through 2017, where analysis data from the Rapid Update Cycle (RUC) and Rapid Refresh (RAP) were available. In total, the dataset used herein contains 18,665 reports. The RAP and RUC were used depending on their availability (the RAP was not operationally implemented until 1 May 2012), in similar fashion to the approach of Bothwell et al. (2014). We acknowledge these models have evolved over time throughout their respective periods of operation. Modeled environmental vertical profiles of wind were taken from the initialization hour RUC/RAP model analysis, at the nearest grid point to the latitude and longitude coordinates of each report. Unlike prior studies that have used the profiles from SPC mesoanalysis, which combines near-surface data from a Barnes

Accepted for publication in *Weather and Forecasting.* DOI 10.1175/WAF-D-21-0136.1.

objective analysis with pressure-level data from RUC/RAP analysis (e.g. Warren et al. 2021; Thompson et al. 2012; Coffer et al. 2019), vertical profiles of wind were created by appending the raw RUC/RAP surface data to the pressure level data. This study does not employ a design such as is suggested in Potvin et al. (2010) to minimize the impacts of contamination from nearby convection by way of spatial offsetting, but it does use the analysis hour recorded by Thompson et al. (2012), which rounds down to better capture the pre-storm environment (for example, a report at 2045 UTC would be represented with a 2000 UTC RAP sounding). Compared to observed soundings, the RUC exhibits a near-surface cool and dry bias and underestimation of CAPE (Thompson et al. 2003), as well as a bias toward stronger lower-tropospheric winds (Coniglio 2012). The RAP model, on the other hand, exhibits a near-surface warm and dry bias (Wade et al. 2018; Coniglio and Parker 2020; Coniglio and Jewell 2021).

Cases were categorized into the following types: right-moving supercell tornado (hereafter RM Tor), right-moving supercell hail (RM Hail), and left-moving supercell hail (LM Hail), with these being either discrete (D) or non-discrete (ND) supercells. Further details regarding the classification of storm mode can be found in Smith et al. (2012). These case types were broken down into bins of report magnitude. The hail data were stratified using the methodology of Johnson and Sugden (2014), such that bins were chosen that do not overlap, in order to ensure meaningful distinction in any signal between categories. Of the bins, the 1.00"–1.75" bin is referenced to as "marginally severe", the 2.00"–3.75" bin as "large", and the ≥4.00" bin as "giant" (Knight and Knight 2001). Tornadoes were also combined into impact-based categories: the EF0–EF1 bin was classified as "weak", the EF2–EF3 bin as "strong", and the EF4–EF5 bin as "violent", such has been colloquialized by Concannon et al. (2000) and many others.

A number of inaccuracies may exist in the dataset used in this study, simply due to the human nature of severe hail reporting. First, location/time biases have been noted with hail reporting (Schaefer and Galway 1981; Baumgardt 2011; Allen and Tippett 2015). Inaccurate size reporting may affect the size bin that reports are put into (Jewell and Brimelow 2009; Schaefer et al. 2004). Moreover, it is possible that severe hail remains unreported in many instances where a tornado is ongoing simultaneously, due to the greater risk posed by the latter. This is to say that severe hail cannot be ruled out with any case in this research that also produced a tornado, and that the impacts

Accepted for publication in *Weather and Forecasting.* DOI 10.1175/WAF-D-21-0136.1.

of this on results may be non-negligible. That said, there is currently no published literature that explores this hypothesis.

There are also known inconsistencies in data collection that may impact this study, as were noted in Warren et al. (2021). For instance, the collection of marginally severe hail for the hazard–storm mode dataset was only carried out in the years 2014–2015; this may affect the true composite hodographs for the smallest size bin. Furthermore, during these two years, the collection of all reports (both hail and tornado) were subjected to a minimum effective bulk wind difference (EBWD Thompson et al. 2007) criteria, which was increased from 20 kt in 2014 to 40 kt in 2015. This may affect the mean composite hodographs of all report types, because instances of reports in environments with weaker EBWD than this threshold would not have been included in the dataset. Finally, due to the nature of reporting, if both hail and tornado were reported from a similar location at a similar time, soundings in this dataset could be duplicated, such that one wind profile is used for both a tornado and a severe hail report. The extent to which these testable biases appear to actually influence our results and conclusions is discussed in Appendix A1.a.

b. Hodograph composites

Composite hodographs were generated from RAP soundings linearly interpolated to a common vertical resolution of 250 m. A number of different compositing techniques have been used in literature. With a ground-relative approach, no transformation of modeled u and v wind is applied to the hodographs before compositing (Markowski et al. 2003; Nowotarski and Jones 2018). While this technique is simple and can reveal information regarding the prevailing wind patterns during convective events, its ability to re-construct the true mean hodograph shape is dubious, since input shear profiles can span a variety of different quadrants and rotations which will smooth and cancel out without a normalization. Rather, depending on the subject of study, two different approaches were employed to composite the hodographs. Where examining the storm-relative wind profile, a rotated storm-relative composite hodograph was created. This was done by first subtracting the estimated storm motion (Bunkers et al. 2000) from the modeled wind profile, then rotating the resulting hodograph such that the direction of the prior estimated storm motion lies along the positive direction of the x-axis (Coniglio and Parker 2020). We reference u_{SR} and v_{SR} as the components resulting from this rotation. While non-rotated storm-relative hodographs lose

Accepted for publication in *Weather and Forecasting.* DOI 10.1175/WAF-D-21-0136.1.

important storm-relative details upon compositing due to their dependence on the cardinal direction of the wind, rotated storm-relative hodographs can be composited regardless of the prevailing wind direction.

Primarily, however, we used a rotated shear-relative approach similar to that done by a number of past studies (Rasmussen and Straka 1998; Bunkers et al. 2006; Parker 2014; Bunkers et al. 2000; Warren et al. 2021) in order to better preserve the actual shape of each hodograph upon compositing. With this method, a shear layer must be selected by which to rotate each input hodograph, such that all input hodographs are rotated so that their shear vector lies along the positive x-axis. We reference u' and v' as the components resulting from this rotation. Though the final composite depends somewhat on which shear layer is chosen, this method has no dependence on the accuracy of an estimated storm motion, the direction of storm motion relative to the shear profile, or the quadrant the shear profile exists in. In accordance with Brown (1993), an optimal composite for a given study ought to use a shear layer which spans the depth of the phenomenon being examined. Because the distinguishing characteristics between hail hodographs and tornadic hodographs appear to include weak shear and a lack of curvature in the lowest few km (Gutierrez and Kumjian 2021; Johnson and Sugden 2014; Kumjian et al. 2019, 2021), the 0–3-km shear vector was chosen arbitrarily for this study. A deeper-layer shear vector, such as was used in Bunkers et al. (2000), Bunkers et al. (2006), Parker (2014), and Warren et al. (2021), would in theory be less optimal due to its lack of focus on the low-level shear structure. Likewise, a 0–1-km shear vector would lack consideration for the upper-level shear structure. This arbitrary selection has precedent (Rasmussen and Straka 1998), and is warranted here, as an "optimal" shear layer for this study lacks definition. The shear-relative hodograph composite was then translated to the origin (Rasmussen and Straka 1998). Rather than taking a low-level mean wind, however, the surface wind will be plotted at the origin to avoid averaging a shear layer that appears to be important per the above literature. The authors strongly encourage the use of this shear-relative composite methodology for similar future studies, in order to prevent any assessments drawn from results that do not faithfully represent the sample hodographs.

Accepted for publication in *Weather and Forecasting.* DOI 10.1175/WAF-D-21-0136.1.

c. Environmental parameters

The kinematic parameters used were calculated from the interpolated modeled u and v component wind for each case. The storm-relative wind was obtained from the rotated storm-relative hodograph, such that a positive v component of storm relative wind blows from the right with respect to storm motion. Values of BWD were calculated for the 0–500-m (BWD005), 0–1-km (BWD01), 0–3-km (BWD03), 0–6-km (BWD06), 0–9-km (BWD09), 0–12-km (BWD012), 1–3-km (BWD13), 1–6-km (BWD16), 1–9-km (BWD19), and 1–12-km (BWD112) layers. The ratios of 0–1 km to 0–6 km BWD (denoted BWD01/06) and 0–1 km to 1–6 km BWD (denoted BWD01/16) were also computed. SRH (m^2 s^{-2}) was calculated for the 0–500-m (SRH005), 0–1-km (SRH01), 0–3-km (SRH03), and 1–3-km (SRH13) layers. For the near-ground layer (0–500 m AGL), the mean, maximum, and surface storm-relative wind in m s^{-1} (SRWmean, SRWmax, SRWsfc) were calculated, as well as the mean and maximum integrated streamwise component of vorticity (SWVmean and SWVmax, s^{-1}):

$$\omega_s = \frac{\nabla \times (\boldsymbol{v} - \boldsymbol{c}) \cdot (\boldsymbol{v} - \boldsymbol{c})}{\|(\boldsymbol{v} - \boldsymbol{c}\|)} \tag{1}$$

Where $\boldsymbol{v}$ is the three-dimensional environmental wind and $\boldsymbol{c}$ is the storm motion.

The "critical angle" (CA) is calculated using the method proposed by Esterheld and Giuliano (2008). The "streamwiseness" ($\widetilde{\omega_s}$, unitless) of horizontal vorticity is calculated by dividing the integrated streamwise component of horizontal vorticity by the integrated total magnitude of the horizontal vorticity in a layer:

$$\widetilde{\omega_s} \equiv \frac{\omega_s}{\omega} \tag{2}$$

This streamwise-to-total vorticity ratio ($\widetilde{\omega_s}$, streamwiseness) is similar to the streamwise-to-crosswise ratio explored in Coffer et al. (2019) to examine tornado environments. But while the streamwise-to-crosswise vorticity ratio approaches infinity when the crosswise vorticity in the layer approaches zero (a relatively common occurrence in tornado environments, per Coffer et al. (2019)), $\widetilde{\omega_s}$ approaches infinity when the shear in the layer approaches zero. Though neither of these are optimal behaviors, we use $\widetilde{\omega_s}$ herein because 1) near-zero low-level shear is rare in tornado environments (Coffer et al. 2020), so an approach to infinity would be rare when the parameter

Accepted for publication in *Weather and Forecasting.* DOI 10.1175/WAF-D-21-0136.1.

is actually useful, and 2) its values are intuitive to the user (e.g. 0.9 means that the vorticity is 90% streamwise). Though this unitless parameter has not, to the authors' knowledge, been used in statistical studies of supercells, the degree to which vorticity is streamwise is still fundamentally important in supercell dynamics (Coffer and Parker 2017). Some of the kinematic calculations were made possible with the help of MetPy (May et al. 2021). A variety of thermodynamic parameters derived from the SPC mesoanalysis, available as part of the hazard–storm mode dataset, were used in this study. These include most-unstable CAPE (MUCAPE), 100 mb mixed-layer CAPE up to 3 km (ML3CAPE), 100 mb mixed-layer LCL (MLLCL), and total precipitable water (PW).

3. Results

a. Hodograph shapes

First, the hodographs of both report types (RM/LM Hail and RM Tor) from all discrete supercells are examined in detail. With the exception of a weak shear layer in the lowest kilometer, the hodographs for severe hail-producing right-moving (RM) supercells are primarily long and straight (Fig. 1 d–f), fitting the conceptual model for splitting supercells (Weisman and Klemp 1986), with considerable spread especially above 6 km (this spread can be expected given the low-level shear-relative compositing approach used). The mean hodograph for marginally severe hail most resembles the mean hodograph found by Kumjian et al. (2019) to be associated with large accumulations of small hail. For all hail sizes, the 0–1-km BWD (on average less than 9 m s^{-1}), was relatively weak compared to the 1–12-km BWD (on average greater than 25 m s^{-1} and increasing with hail size). The increase in shear above 1 km appeared to be most important for larger hail. Specifically in RM supercells, 0–1-km BWD increased by 2.3 m s^{-1} from small to giant hail, 0–12-km BWD increased by 2.7 m s^{-1}, but the largest difference was found in the 1–12-km BWD at 4.0 m s^{-1}. Heidke skill scores (HSS) were calculated for each shear layer in order to determine the layer that "best" discriminates between hail size bins (Hyvärinen 2014). The HSS has been found to be effective in rare event forecasting (Doswell et al. 1990). The 0–500-m BWD performed best at distinguishing between marginally severe and large hail with an HSS of 0.17, while all shear layers were very poor indicators (HSS < 0.1) of giant hail (Tables 1). This is no surprise; though we noted minor differences, the hodographs for all hail sizes from discrete, RM supercells are still very similar (Fig. 2). The hodographs for the left-moving (LM) counterparts (Fig. 1 a–c)

Accepted for publication in *Weather and Forecasting*. DOI 10.1175/WAF-D-21-0136.1.

displayed similar differences between the size bins, with the most notable being an increase in shear above 1 km with increasing hail size. In general, compared to the RM supercell hodographs, these featured a gradual but prominent backing of the mid-level shear vector and weaker 0–1-km BWD. The composites of LM supercells also resembled those found by Bunkers (2002).

TABLE 1. The 10 most skillful environmental predictors (based on HSS) of (left) large hail versus marginally severe hail, and (right) giant hail versus large hail. The first and second columns contain the median values of each variable for the given categories. The third and forth columns contain the skill score and critical threshold respectively. Units for the variables can be found in section 2.c.

	1.00–1.75"	2.00–3.75"	HSS	Thresh
SRH01	71	113	0.18	72
SWVmax	0.009	0.013	0.17	0.009
BWD005	4.2	5.8	0.17	4.4
SRWmax	15.5	17.1	0.16	15.8
SRH005	40	64	0.16	81
SWVmean	0.006	0.008	0.15	0.008
SRWmean	14.4	15.6	0.15	14.8
BWD01	6.7	8.5	0.15	7.0
SRH03	168	217	0.14	170
CA	75	88	0.12	76

	2.00–3.75"	≥4.00"	HSS	Thresh
BWD19	26.1	27.0	0.06	32.5
SRH03	217	220	0.05	371
BWD03	17.0	17.4	0.04	24.3
SRWmean	15.6	16.0	0.04	16.8
SRH01	113	132	0.04	222
BWD13	12.1	12.6	0.03	23.7
BWD09	29.6	31.1	0.03	34.7
BWD01/06	20.4	21.6	0.03	0.90
BWD16	20.4	21.6	0.03	23.1
SWVmax	0.013	0.015	0.03	0.028

TABLE 2. The 10 most skillful environmental predictors (based on HSS) of (left) strong tornadoes versus weak tornadoes, and (right) violent tornadoes versus strong tornadoes. The first and second columns contain the median values of each variable for the given categories. The third and forth columns contain the skill score and critical threshold respectively. Units for the variables can be found in section 2.c.

	EF0–1	EF2–3	HSS	Thresh
SRH005	115	221	0.28	233
SRH01	173	317	0.27	352
BWD01	11.6	17.1	0.27	18.2
SWVmean	0.014	0.022	0.26	0.025
SRWsfc	15.2	19.5	0.26	19.7
BWD005	8.4	12.5	0.25	14.8
SRH03	254	396	0.25	407
BWD03	17.9	23.0	0.25	23.3
SRWmean	15.8	18.9	0.24	18.9
SRWmax	17.2	20.6	0.24	20.5

	EF2–3	EF4–5	HSS	Thresh
BWD03	23.0	26.3	0.19	31.7
SRWsfc	19.5	22.9	0.19	25.5
BWD01	17.1	19.8	0.19	27.3
SRH005	221	250	0.15	471
SRWmax	20.6	23.1	0.14	25.36
SRWmean	18.9	20.1	0.14	24.32
SRH01	317	340	0.13	616
BWD06	29.8	32.9	0.12	37.8
SRH03	396	498	0.12	852
SRH13	83	98	0.11	149

Accepted for publication in *Weather and Forecasting.* DOI 10.1175/WAF-D-21-0136.1.

TABLE 3. The 10 most skillful environmental predictors (based on HSS) of significant-severe hail versus significant tornadoes. The first and second columns contain the median values of each variable for the given categories. The third and forth columns contain the skill score and critical threshold respectively. Units for the variables can be found in section 2.c.

	Hail ≥2.00"	Tor ≥EF2	HSS	Thresh
SRH005	65	226	0.47	175
SWVmean	0.009	0.022	0.47	0.019
BWD01	8.5	17.5	0.45	15.4
SRH01	115	317	0.44	270
SWVmax	0.014	0.032	0.43	0.028
BWD005	5.9	12.7	0.42	13.3
BWD01/16	0.42	0.90	0.42	0.78
BWD01/06	0.36	0.59	0.39	0.53
SRH03	217	399	0.37	330
BWD03	17.1	23.2	0.36	20.8

To better explore the differences between hodographs capable of significant-severe hail in a RM supercell versus a LM supercell, their respective rotated storm-relative hodographs were also examined. Some differences could be found between the two (Fig. 3 a and d). Near the surface, LM supercells that produced significant-severe hail ingested the opposite sign of horizontal vorticity (streamwise) than was available aloft (antistreamwise), consistent with Bunkers (2002). This is due in large part to the tendency of low-level winds to naturally veer with height in the northern hemisphere due to the combined effects of friction and the Coriolis force. In addition, near-surface storm-relative inflow was slightly stronger for LM supercells than for RM supercells. In the mid- and upper-levels, storm-relative flow was also marginally stronger for left-movers. In addition, the orientation of the storm-relative wind profile was quite different, with LM supercells subjected to mid- and upper-level winds directed sharply to the right-of-motion, rather than more forward, as was the case with RM supercells. Due to the impact of storm-relative winds on hydrometeor transport (Lemon and Doswell 1979; Rasmussen and Straka 1998), this suggests that LM hail-producing supercells tend to move into more undisturbed air, whereas a RM supercell may move more along or into its forward-flank downdraft. Future work may be necessary to determine if this actually affects the hail growth process, and if the structures of severe hail-producing RM and LM supercells are significantly different.

Accepted for publication in *Weather and Forecasting.* DOI 10.1175/WAF-D-21-0136.1.

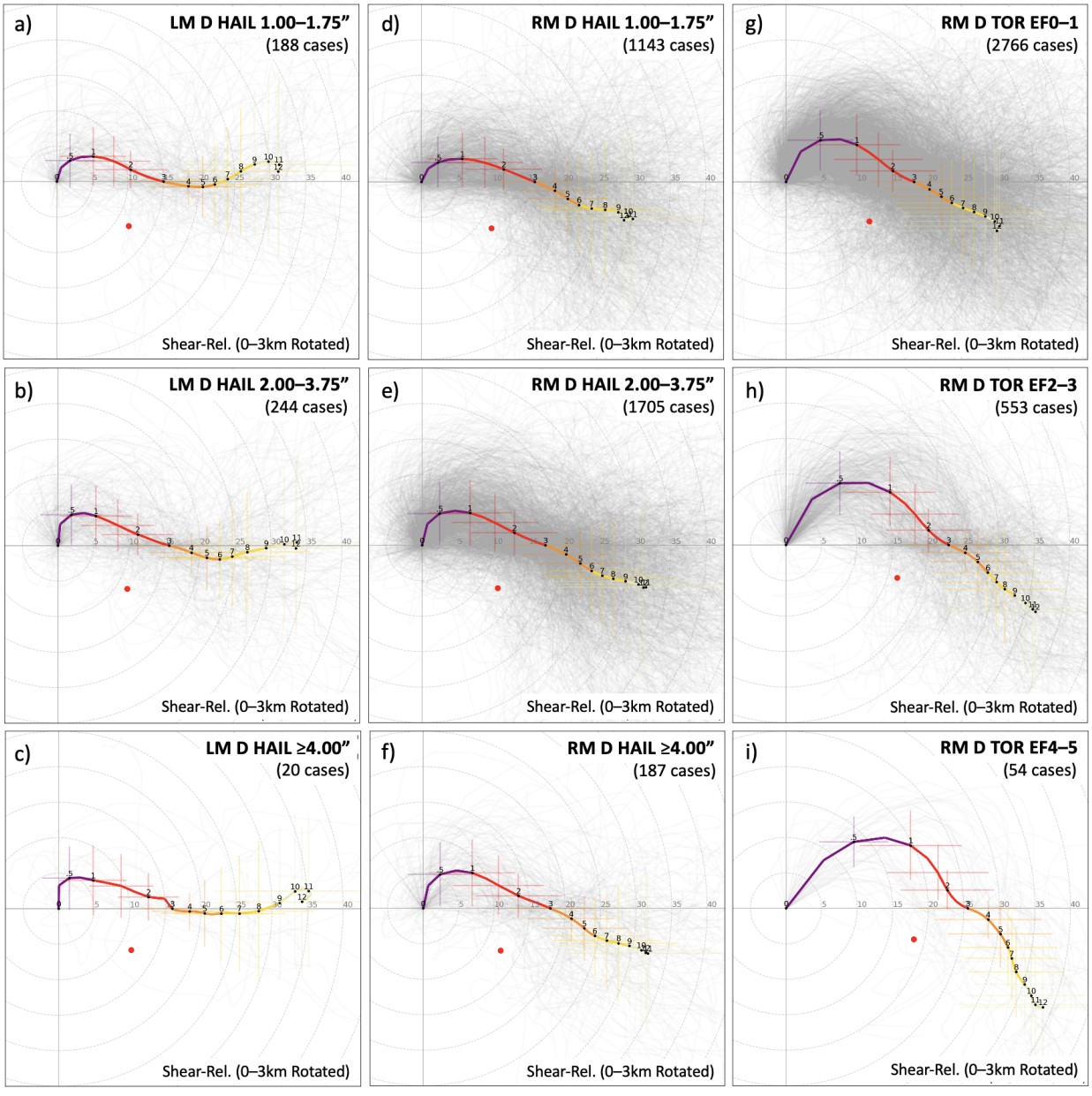

FIG. 1. Composite shear-relative hodographs for LM (a–c) and RM (d–f) severe hail-producing supercells, and RM tornado-producing supercells (g–i). The colored line is the mean composite hodograph (purple is 0–1 km, red is 1–3 km, orange is 3–6 km, yellow is 6–9 km, and light yellow is 9–12 km), while the grey lines are each individual hodograph considered in the composite. The colored bars denote the standard deviation of the wind components at each level (500–2000 m at every 500 m, then 2000–12000 m at every 1000 m). The red dot marks the Bunkers estimated storm motion. Winds are in m s^{-1}.

Accepted for publication in *Weather and Forecasting*. DOI 10.1175/WAF-D-21-0136.1.

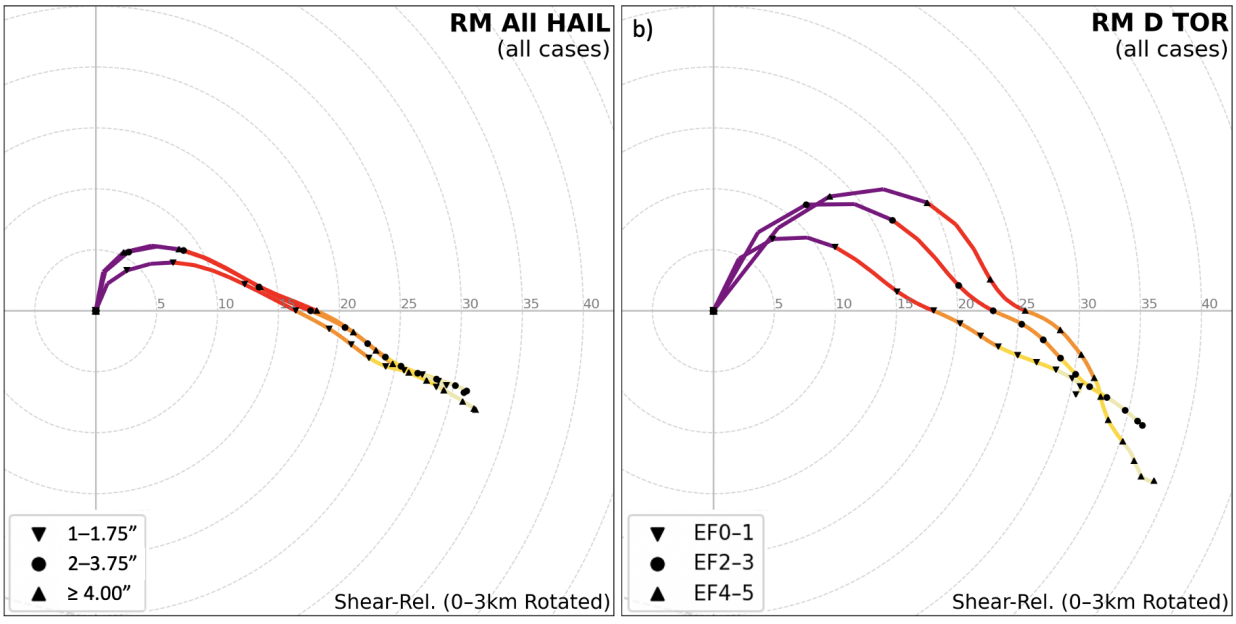

FIG. 2. Composite shear-relative hodographs for (left) all discrete severe hail-producing RM supercells (with the hodograph for hail 1.00–1.75" marked by downward-pointing triangles, 2.00–3.75" marked by circles, and greater than or equal to 4.00" marked by upward-pointing triangles), and (right) all discrete tornado-producing supercells (with the hodograph for EF0–1 tornadoes marked by downward-pointing triangles, EF2–3 marked by circles, and EF4 or stronger marked by upward-pointing triangles). The colored line is the mean composite hodograph (purple is 0–1 km, red is 1–3 km, orange is 3–6 km, yellow is 6–9 km, and light yellow is 9–12 km). Winds are in m s^{-1}.

The hodographs for tornadic supercells (Fig. 1 g–i) displayed dramatically different shapes than those that produced severe hail. The weakly tornadic hodograph appeared most like the severe hail-producing hodographs, but with a stronger median 0–1-km BWD of 11.6 m s^{-1}. The strongly tornadic hodograph possessed 0–1-km BWD of 17.1 m s^{-1} with a proportionately large 0–500-m BWD; this affirms work by Coffer et al. (2020) that significant tornadoes tend to have high concentrations of shear (thus storm-relative helicity) in the lowest half-kilometer. The violently tornadic hodograph continues this trend, with 0–1-km BWD of 19.8 m s^{-1}, becoming comparable in magnitude with the 1–6-km BWD (with 1–6-km BWD very close in magnitude at 20.8 m s^{-1}). The shear above 1 km strengthened with tornado intensity, with 1–12-km BWD again increasing the most between bins, with violent tornadoes possessing a median of 6.7 m s^{-1} stronger shear in this layer than was found with weak tornadoes. Of all layers, the 0–6-km BWDs displayed

Accepted for publication in *Weather and Forecasting*. DOI 10.1175/WAF-D-21-0136.1.

the largest separation in medians between weak and violent tornadoes, at 9.0 m s^{-1}; however, considerable spread does exist especially above 6 km. When HSS was considered, the 0–1-km BWD performed best at distinguishing between weak and strong tornadoes with an HSS of 0.27, while the 0–3-km BWD performed best at distinguishing between strong and violent tornadoes with an HSS of 0.19. In fact, of all parameters tested, the 0–3-km BWD carried the greatest skill at distinguishing between strong and violent tornadoes. The mean violent tornado hodograph also displayed a slight backing of the shear vector above 2 km (a feature which also appears to a lesser degree in the strong tornado hodograph). Backing aloft has not been traditionally associated with significant tornadoes, but can be seen in some past hodograph composites (e.g. Maddox 1976; Bunkers et al. 2006; Coniglio and Parker 2020; Nowotarski and Jensen 2013) and discussed more in depth in more recent literature (for instance by Parker 2017; Warren et al. 2021). The caveat to this observation is that the small sample size (54) of violent tornadoes used in this study may introduce more structure in the hodograph than would appear with a larger sample of cases. Though there is no way to test this conclusively, we include in the Appendix a test which suggests that this backing aloft, though also explored in past literature, may be an artifact of this small sample size. Overall, compared to the severe hail-producing hodographs (Fig. 1 a–f), the mean significantly tornadic hodographs feature stronger low- and deep-layer shear, and a greater fraction of low-level shear relative to the shear above 1 km. Also compared to severe hail, tornado intensity appears much more tied to, and thus predictable by, the shear profile (Fig. 2), which supports the extensive body of literature on the importance of wind shear in forecasting significant tornadoes.

Lastly, the composite hodographs responsible for severe hail and tornado reports from discrete supercells were compared to the composite hodographs from non-discrete supercells (Fig. 3 b, c, e, and f). The differences between hodographs was greatest in the lowest-magnitude report bins, becoming less pronounced with larger hail / stronger tornadoes (not shown). Between the two modes, non-discrete cases featured notably stronger shear in the lowest 1 km, as well as more veering with height. Especially for the tornadic cases, this may mean that more favorable shear profiles are necessary to counteract any less favorable local thermodynamics caused by cell interactions or stratiform precipitation in the vicinity of mesoscale convective systems. However, aside from the association of stronger low-level shear with enhanced mesoscale convective system

Accepted for publication in *Weather and Forecasting*. DOI 10.1175/WAF-D-21-0136.1.

maintenance (Rotunno et al. 1988), the reasons or impacts of the difference in hodograph structure are unclear.

b. Shear parameters

Next, we will explore a number of different shear parameters, and how they performed in differentiating between the hazards and their magnitudes in all discrete supercells. Though all predictors were tested, only the top 10 most skillful (based on HSS) are displayed in Tables 1, 2, and 3, along with their critical threshold (the value that shows most skill in distinguishing between the two samples) and the median values of each sample. As with all bulk statistical studies, it is important to remember that an association is not a causation, and that the average relationship between parameter and predictor may not hold on a case-by-case basis.

First, the BWD of various layers were compared between the magnitudes of the hail and tornado reports, with some of the most commonly used layers illustrated in Fig. 4 (a–c and d–f). Of the layers, 0–1-km rather unsurprisingly displayed the most skill in differentiating between weak and strong tornadoes, echoing Rasmussen and Straka (1998). Both 0–3-km and 0–1-km BWD show comparable but relatively weak skill (HSS = 0.19) in discriminating between strong and violent tornado environments. There was no BWD that displayed similarly promising predictability for hail sizes, and of all layers, the 0–6-km BWD consistently ranked among the lowest. These BWD parameters were then compared to determine whether or not particular layers could differentiate between environments conducive to significant-severe hail and significant tornadoes (Fig. 4 g–i). The 0–1-km BWD displayed the most promising capability of differentiating between the two with a rather strong HSS of 0.45 at a threshold of 15.4 m s^{-1}. Similarly, 0–6-km BWD was stronger for tornadic supercells, while 1–6-km BWD was about the same.

Accepted for publication in *Weather and Forecasting.* DOI 10.1175/WAF-D-21-0136.1.

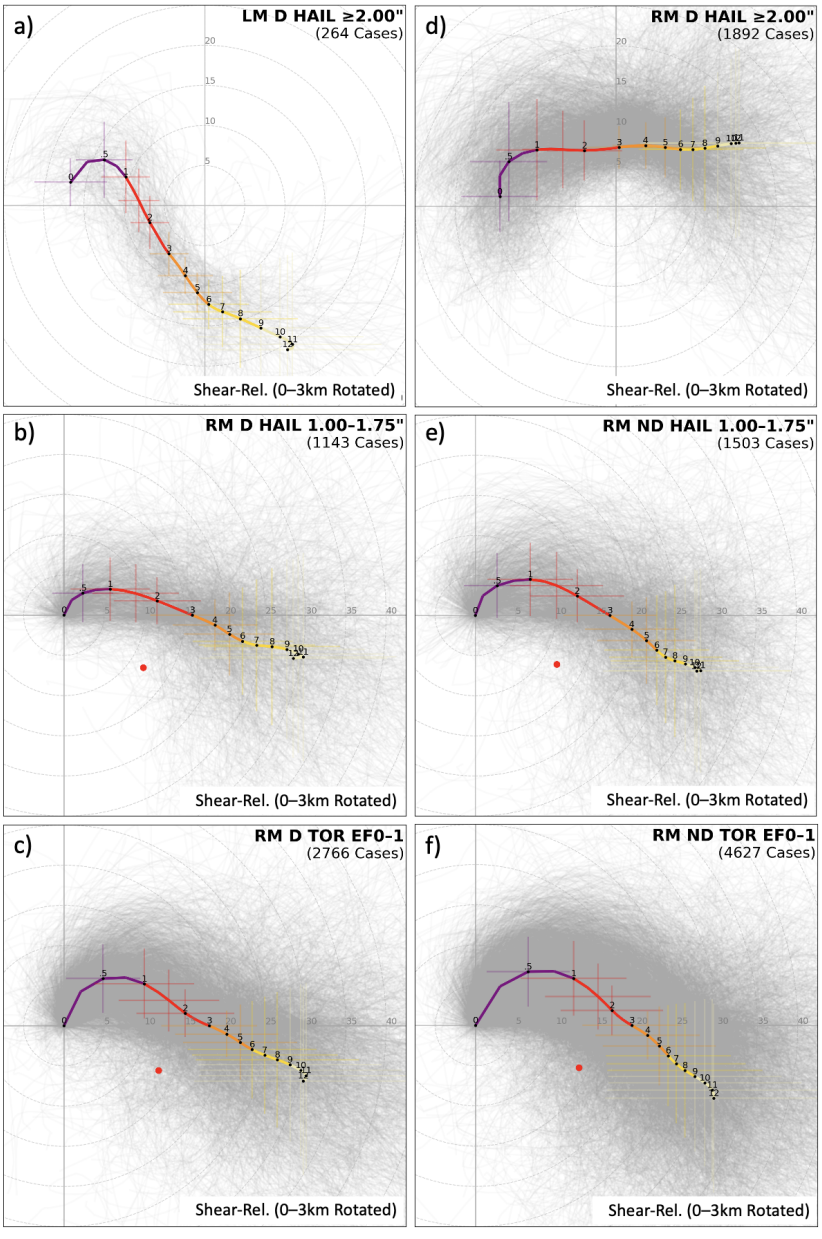

FIG. 3. Composite storm-relative hodographs for significant-severe hail-producing LM (a) and RM (d) supercells, composite shear-relative hodographs for RM discrete (b) and non-discrete (e) severe hail-producing supercells, and composite shear-relative hodographs for RM discrete (c) and non-discrete (f) weak tornado-producing supercells. The colored line is the mean composite hodograph (purple is 0–1 km, red is 1–3 km, orange is 3–6 km, yellow is 6–9 km, and light yellow is 9–12 km), while the grey lines are each individual hodograph considered in the composite. The colored bars denote the standard deviation of the wind components at each level. The red dot marks the Bunkers estimated storm motion. Winds are in m s^{-1}.

Accepted for publication in *Weather and Forecasting*. DOI 10.1175/WAF-D-21-0136.1.

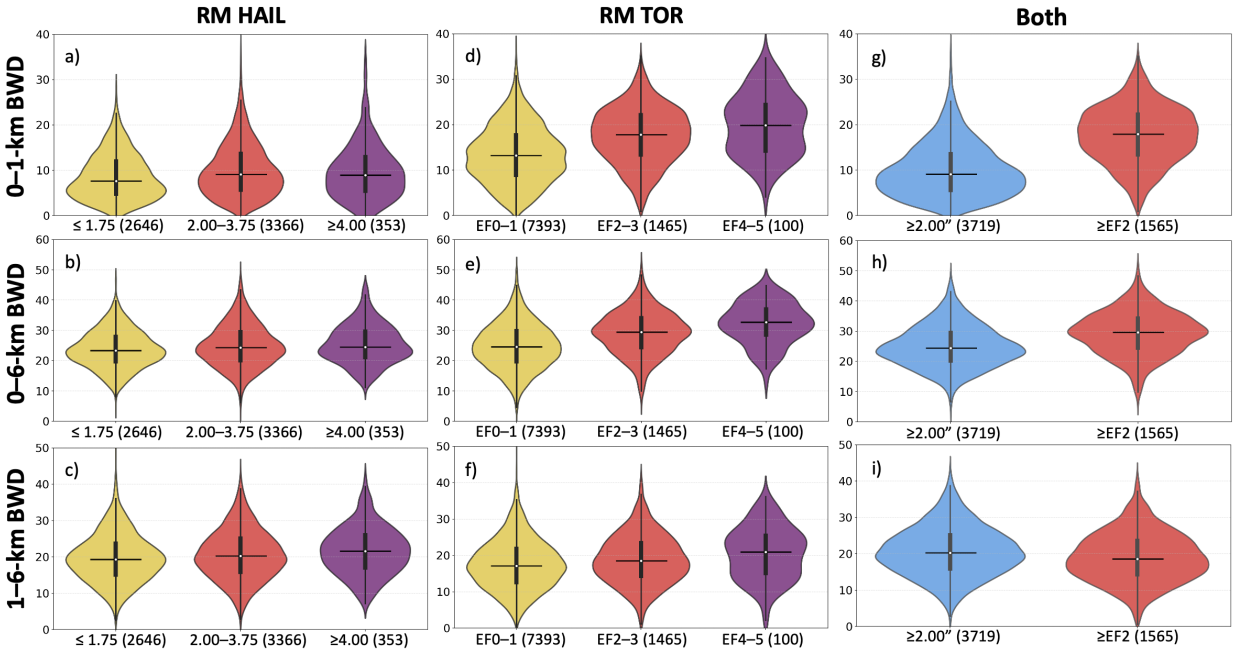

FIG. 4. Violin plots of bulk wind difference (m s^{-1}) over (from top to bottom) 0–1 km, 0–6 km, and 1–6 km for RM severe hail-producing supercells by increasing maximum hail size (a–c) and tornado-producing supercells by increasing EF rating (d–f), and a comparison for significant-severe hail and significant tornadoes (g–i). The thin black vertical line represents the range of data between the lower and upper adjacent values (non-outlier range), the thick black vertical line represents the interquartile range, and the black horizontal line denotes the median.

Accepted for publication in *Weather and Forecasting*. DOI 10.1175/WAF-D-21-0136.1.

To investigate the tendency for significantly tornadic supercells to possess a greater proportion of 0–1-km BWD than significant hail-producing supercells, the ratios of 0–1 km to 1–6 km BWD (BWD01/16) and 0–1 km to 0–6 km BWD (BWD01/06) were assessed (Fig. 5). BWD01/16 exhibited slightly lower skill than low-level BWD and SRH, but still distinguished between the two hazards with an HSS of 0.42. This was closely followed in skill by BWD01/06. The 1–6-km BWD was stronger than the 0–1-km BWD in only 55% of significant tornado cases, as opposed to 89% of significant hail cases. Using a 2D kernel density estimate, various shear parameter spaces were compared, with the two displaying the furthest separation of maxima shown in Fig. 6. Though the use of simply BWD01 and BWD01/16 was very effective in separating the samples of significant-severe hail and significant tornadoes, the use of BWD06 alongside BWD01 may be similarly effective.

SRH was also compared between the different categories of tornado and hail reports for the 0–500-m, 1–3-km, and 0–3-km layers (Fig. 7). Of the three layers, 0–500-m SRH (followed by 0–1-km SRH, not pictured) displayed the greatest skill in differentiating between all tornado rating bins (Fig. 7 a–c), with higher SRH found in stronger tornado cases. This is consistent with the findings of Coffer et al. (2019), which is unsurprising given that their study also used the SPC hazard–storm mode dataset. Though 0–500-m SRH displayed the best skill (HSS of 0.28) by a very small margin, 0–500-m SRH, 0–1-km SRH and 0–1-km BWD performed comparably as the best predictors tested in discriminating between weak and strong tornadoes. Low-level SRH showed marginal skill in distinguishing between marginally severe and large hail, but, like the shear parameters, was generally useless for differentiating between large and giant hail (Fig. 7 d–f). SRH was also compared between significant-severe hail and significant tornadoes (Fig. 7 g–i). Similar to 0–1-km BWD, 0–500-m SRH (not pictured) displayed marginally stronger skill in differentiating between hail and tornado environments with an HSS of 0.47, and is the single best discriminating parameter between the two significant hazards that we examined.

Various less traditional properties of the low-level inflow were also tested, including mean 0–500-m SWV (s^{-1}), max 0–500-m SWV (s^{-1}), mean 0–500-m storm-relative wind (m s^{-1}), max 0–500-m storm-relative wind (m s^{-1}), and surface storm-relative wind (m s^{-1}). 0–1-km BWD and mean 0–500-m storm-relative wind and SWV show comparable skill to low-level SRH at distinguishing strong from weak tornado environments. In addition to the 0–3-km BWD, the

Accepted for publication in *Weather and Forecasting.* DOI 10.1175/WAF-D-21-0136.1.

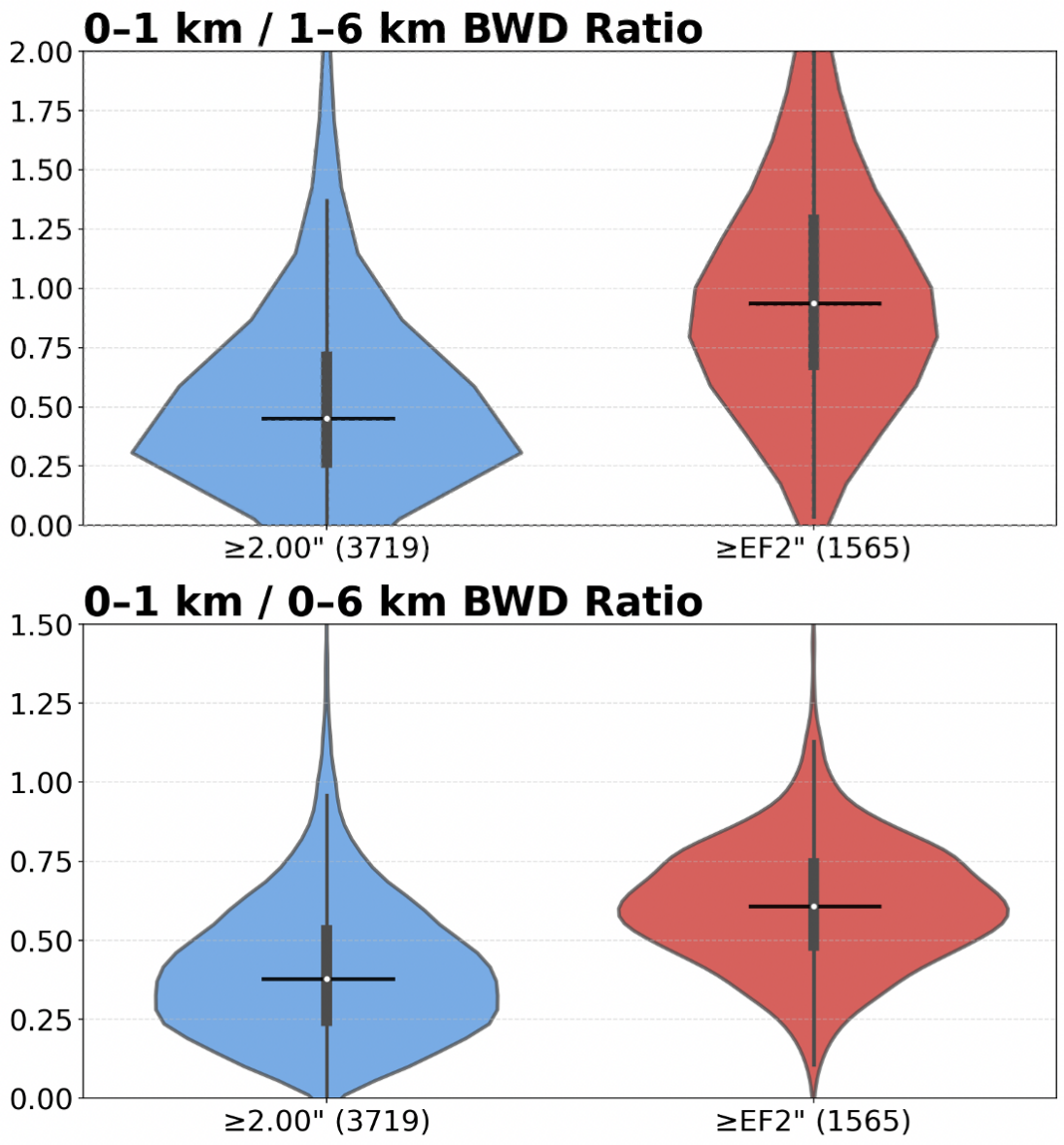

FIG. 5. Violin plots of the ratio of 0–1-km to 1–6-km bulk wind difference (unitless) for RM supercells producing significant-severe hail and significant tornadoes. The thin black vertical line represents the range of data between the lower and upper adjacent values (non-outlier range), the thick black vertical line represents the interquartile range, and the black horizontal line denotes the median.

surface storm-relative wind also showed weak skill at distinguishing between strong and violent tornado environments—interestingly, these were the two most skillful predictors, both marginally better than 0–500-m SRH. Maximum 0–500-m storm-relative wind and SWV displayed comparable

Accepted for publication in *Weather and Forecasting*. DOI 10.1175/WAF-D-21-0136.1.

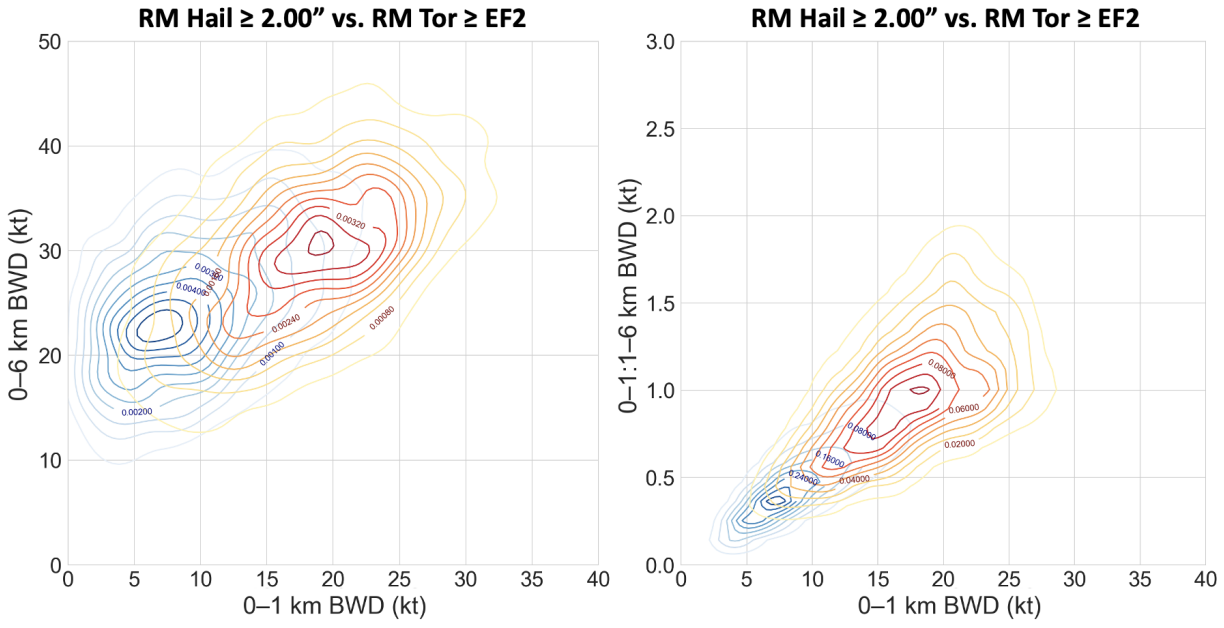

FIG. 6. 2D kernel density estimate (kernel bandwidth of 1.3) of significant-severe hail (blue) and significant tornado (red), using the 0–1-km BWD versus the 0–6-km BWD (left), and the 0–1-km BWD versus the 0–1-km to 1–6-km BWD ratio (right). Probability density is contoured at an interval of 0.0005 (left) and 0.005 (right)

skill to low-level SRH and BWD at distinguishing between marginally-severe and large hail, but these parameters all performed very poorly at distinguishing between large and giant hail.

The critical angle (Esterheld and Giuliano 2008) has become the standard for estimating the "streamwiseness" of the low-level horizontal vorticity (the degree to which the vorticity is streamwise). Given the results of Esterheld and Giuliano (2008), as well as our understanding that more $\widetilde{\omega_s}$ is more favorable for strong low-level mesocyclones (Coffer and Parker 2017), we would expect stronger tornadoes to be associated with critical angles closer to 90 degrees. However, the opposite relationship was found, with critical angles becoming *farther* from 90 degrees as tornado rating increased (Fig. 8). This result contradicts the accepted operational use of critical angle, but is consistent with findings from Coffer et al. (2019) (whose study this dataset overlaps). As noted in Coffer et al. (2019), low-level RAP modeled wind fields may play a role in the direction of the low-level shear, affecting the critical angle in some scenarios. However, the authors suspect that the small sample of 65 Oklahoma supercells examined in Esterheld and Giuliano (2008) was simply not representative of all significant tornado environments. Indeed, Coniglio and Parker (2020) found

Accepted for publication in *Weather and Forecasting*. DOI 10.1175/WAF-D-21-0136.1.

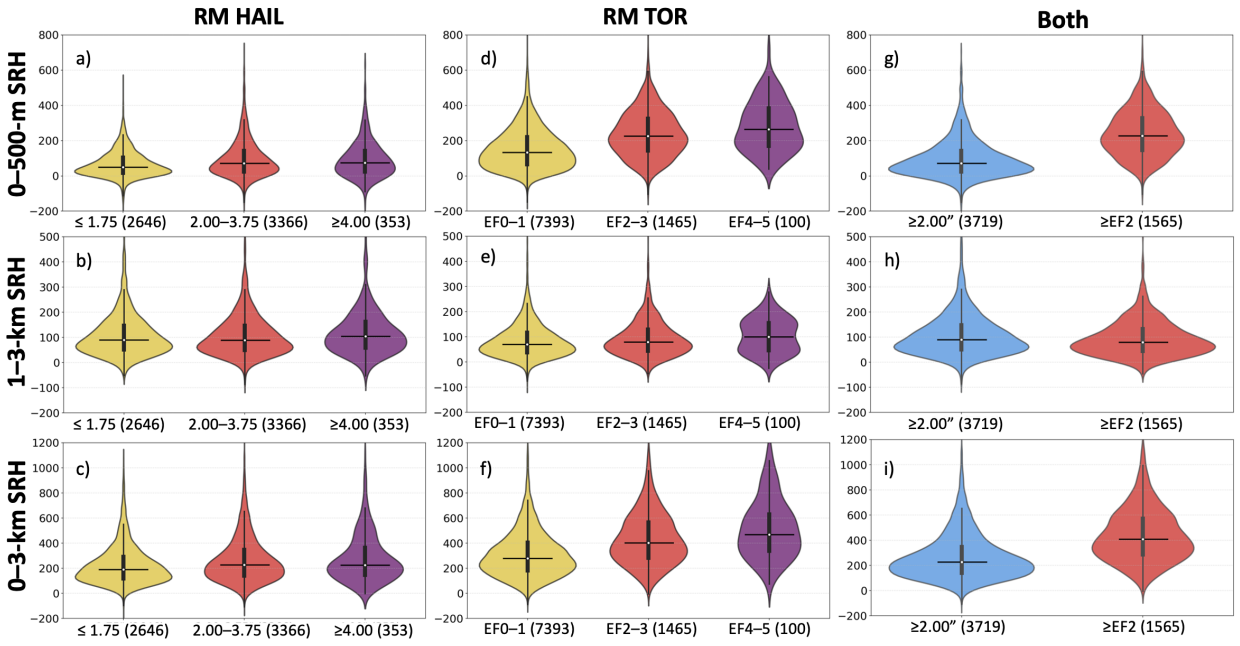

FIG. 7. Violin plots of storm-relative helicity (m^2 s^{-2}) over (from top to bottom) 0–500 m, 1–3 km, and 0–3 km for RM severe hail-producing supercells by increasing maximum hail size (a–c) and tornado-producing supercells by increasing EF rating (d–f), and a comparison for significant-severe hail and significant tornadoes (g–i). The thin black vertical line represents the range of data between the lower and upper adjacent values (non-outlier range), the thick black vertical line represents the interquartile range, and the black horizontal line denotes the median.

that even amongst primarily Central Plains-based supercells, a larger sample of observed cases did not display a significant difference in critical angles between weak and significant tornadoes. It is important to recognize that critical angle is only an estimation of $\widetilde{\omega_s}$. Because it relates the horizontal vorticity of the 0–500-m layer to the surface wind, its ability to faithfully estimate the $\widetilde{\omega_s}$ of either the 0–500-m wind or the surface wind is compromised. Considering its design alone, the authors do not recommend using critical angle to estimate the $\widetilde{\omega_s}$ of the low-level vorticity. Given these results (as well as other recent publications), we strongly caution against associating critical angles near 90 degrees with more favorable tornadic environments.

Rather than using a parameter like critical angle to estimate streamwiseness, the authors encourage the use of $\widetilde{\omega_s}$ itself (a fundamental property of the storm-relative wind). Unlike critical angle, 0–500-m $\widetilde{\omega_s}$ performs as expected (Fig. 8), with stronger tornadoes possessing more purely streamwise vorticity (values near 1.0). That said, we caution that neither parameter shows skill in

Accepted for publication in *Weather and Forecasting*. DOI 10.1175/WAF-D-21-0136.1.

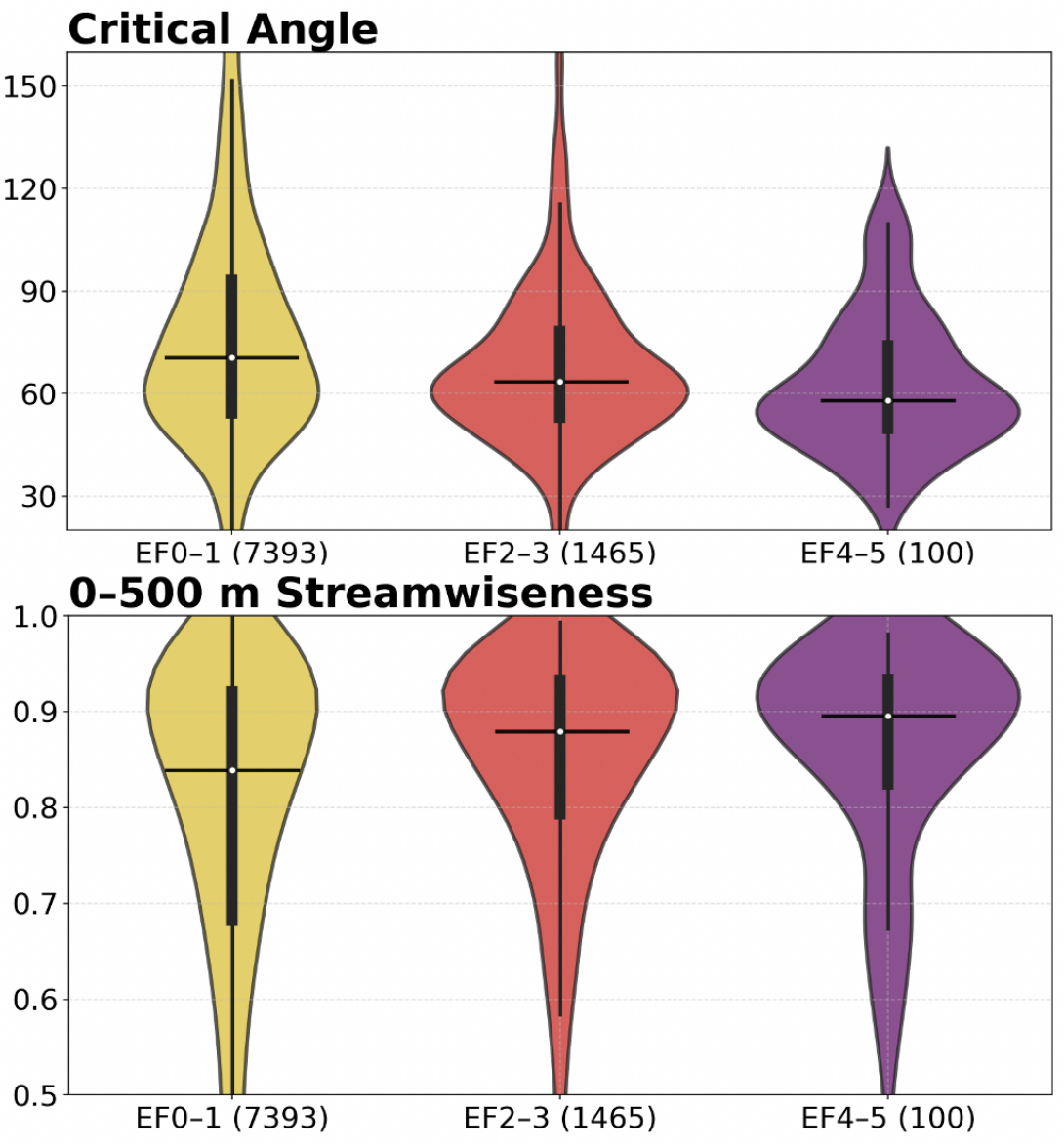

FIG. 8. Violin plots of (top) critical angle (degrees) and (bottom) streamwiseness of the 0–500-m horizontal vorticity (unitless) for all discrete tornado ratings. The thin black vertical line represents the range of data between the lower and upper adjacent values (non-outlier range), the thick black vertical line represents the interquartile range, and the black horizontal line denotes the median.

predicting tornado strength. A property of $\widetilde{\omega_s}$ is that it may approach 0 or 1 as the shear becomes negligible in the layer in which it is calculated. This may potentially mislead in operations, but this is not a design flaw; it is up to the forecaster to recognize that the $\widetilde{\omega_s}$ of vorticity becomes irrelevant when there is no vorticity.

Accepted for publication in *Weather and Forecasting*. DOI 10.1175/WAF-D-21-0136.1.

Lastly, the vertical profiles of storm-relative wind (u_{SR} and v_{SR}) were compared between the magnitudes of both report types (Fig. 9). Among tornadic cases (Fig. 9 d–f), u_{SR} (storm-relative wind perpendicular to storm motion) increased in the lowest 2 km from weak to violent tornadoes. In the upper levels, winds veered to the right of the storm's motion considerably with increasing tornado rating. Storm-relative wind opposing storm motion (in the -v_{SR} direction) increased in the layer below 500 m with increasing tornado rating, while winds in the middle and upper levels displayed only minor differences. The magnitude of the storm-relative wind displayed noticeable differences only below 500 m, with higher-rated tornadoes displaying stronger storm-relative winds especially below 500 m. As with tornadic cases, hail cases (Fig. 9 a–c) displayed a similar increase in perpendicular storm-relative winds in the lowest 2 km from marginally severe to giant hail, with a slight tendency for more rightward veering in the upper levels. Unlike tornadic storms, v_{SR} showed little change between hail sizes. This may support findings by Dennis and Kumjian (2017), Kumjian and Lombardo (2020), and Kumjian et al. (2021) who found that a stronger v-component of shear in the lowest 3 km for a given u-component shear tended to decrease hail production. Thus, a relatively weak meridional component of low-level shear is necessary for hail production. The profile for giant hail closely resembled that found by Gutierrez and Kumjian (2021) to be associated with hail larger than 6.00", suggesting that the signal they identified still applies in a larger sample size.

When comparing storm-relative wind profiles between significant-severe hail and significant tornadoes (Fig. 9 g–i), there are several differences. A much larger negative u_{SR} (directed to the left of storm motion) exists within significantly tornadic storms than significant hail-producing storms, to the point where there is almost no overlap between the interquartile ranges of both samples in the lowest 1 km. The significant tornado cases also exhibit a substantially further positive/rightward u_{SR} in the middle and upper levels. This is likely indicative of stronger ground-relative veering with height. v_{SR} showed some small increase near the surface for the tornadic cases, with a faster rate of change of storm-relative wind with height. These differences are not readily apparent by assessing only the magnitude of the storm-relative wind, so the authors encourage this component-based analysis in future studies and data visualization.

Accepted for publication in *Weather and Forecasting.* DOI 10.1175/WAF-D-21-0136.1.

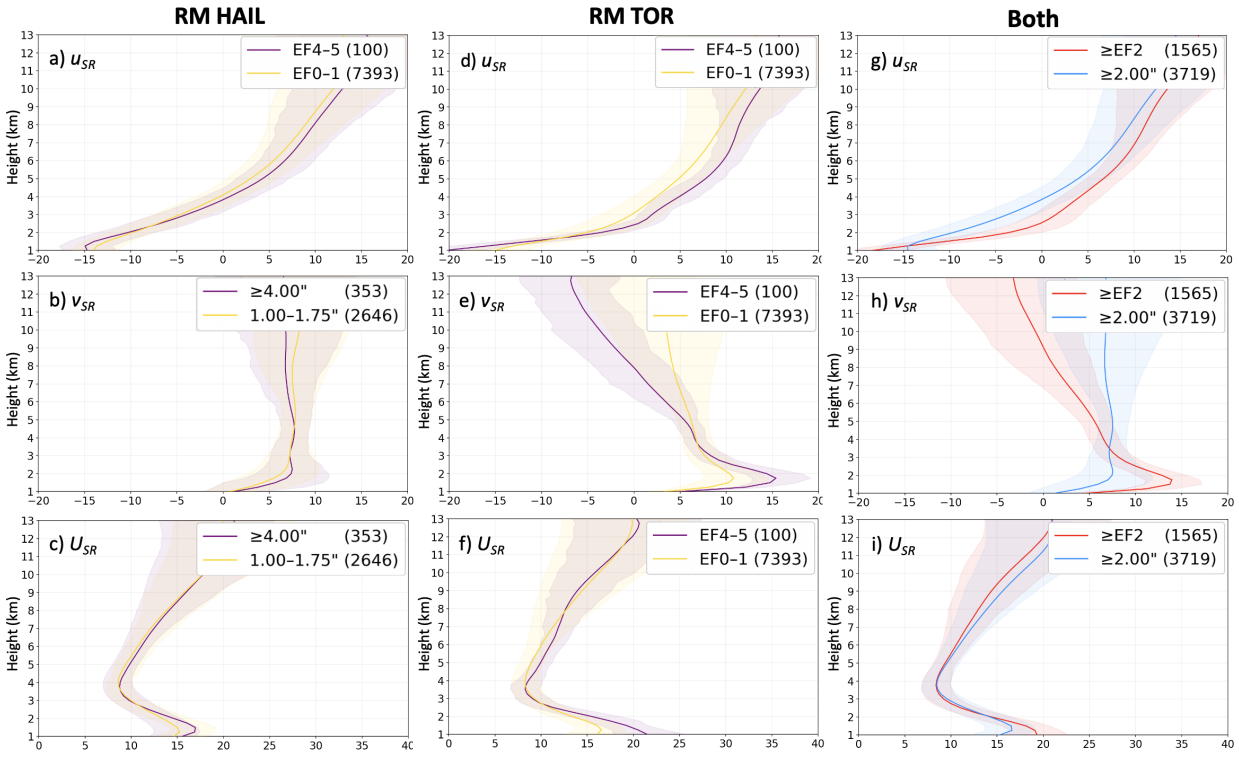

FIG. 9. Plots of the mean storm-relative u-component (a), v-component (b), and wind speed (m s^{-1}) with height for RM severe hail-producing supercells by increasing maximum hail size (1) and tornado-producing supercells by increasing EF rating (2), and a comparison for significant-severe hail and significant tornadoes (3). The colored lines denote the mean of the winds, while the shading denotes the interquartile range. The storm-relative wind components were calculated after the storm-relative rotation of the hodograph, such that u_{SR} is parallel to storm motion (with positive values in the direction of storm motion), and v_{SR} is perpendicular to storm motion (with positive values to the left of storm motion). Shading represents the interquartile range of wind.

c. Impact of thermodynamics on hodograph shapes

Finally, we explore the impact of some commonly used thermodynamic variables on the mean hodographs associated with significant hail and significant tornadoes. The variables examined (MUCAPE, ML3CAPE, MLLCL, and PW) were chosen to gain insights from both the buoyancy profile and the moisture profile. All variables were partitioned into "low" and "high" thresholds arbitrarily, such that could be used consistently between tornado and hail while also balancing sample size for the respective populations. MUCAPE was partitioned into MUCAPE < 1000 J kg^{-1} [the currently accepted threshold for high-shear, low-CAPE environments (Schneider et al.

Accepted for publication in *Weather and Forecasting*. DOI 10.1175/WAF-D-21-0136.1.

2006)] and MUCAPE > 3000 J kg^{-1}. ML3CAPE was partitioned into ML3CAPE < 25 J kg^{-1} and ML3CAPE > 125 J kg^{-1}. MLLCL was partitioned into MLLCL < 750 m and MLLCL > 1500 m. PW was partitioned into PW < 1.00" and PW > 1.75".

For significant tornado cases, MUCAPE (Fig. 10e) and ML3CAPE (Fig. 10f) displayed nearly identical relationships, namely an increase in low-level shear where CAPE was low, and vice versa. Of particular note, the low-CAPE sample of significant tornadoes produced a mean hodograph with stronger low-level shear than the mean hodograph for all violent tornadoes, while the high-CAPE sample of all significant tornadoes was nearly identical to the mean hodograph for all weak tornadoes. The low-CAPE sample was generally found in the Southeast U.S., while the high-CAPE sample spanned much of the Central Plains (Fig. 11e). These samples were also offset seasonally, with high-CAPE cases generally occurring from April through June while low-CAPE cases peaked during the winter and early spring months (Fig. 12e). The difference in seasonal synoptic baroclinicity may explain the difference in shear between these two samples. MLLCL height (Fig. 10g) showed an even more notable difference between hodographs in the same fashion as CAPE, where lower LCLs were associated with much stronger low-level shear than higher LCLs. This should not be surprising given the LCL's relationship with the depth of the mixed layer; high LCLs are indicative of a well-mixed low-level atmosphere, where the bulk wind difference over the depth of the boundary layer is naturally less. PW (Fig. 10h) displayed the most pronounced difference in mid- and upper-level hodograph structure of the four variables, with the high-PW hodograph featuring the weakest deep-layer shear of the samples and the low-PW hodograph featuring comparatively stronger shear above 1 km. The high-PW sample also displayed the most veering of the shear vector with height of the samples, while the low-PW sample displayed the most backing. The weak tornado cases (not shown) followed the same patterns, but with generally weaker low-level and deep-layer shear (as expected given prior results). These samples were generally separated in location (Fig. 11h), as well as time (Fig. 12h), with higher PW cases peaking about a month later but with a long trail into the summer months.

Accepted for publication in *Weather and Forecasting.* DOI 10.1175/WAF-D-21-0136.1.

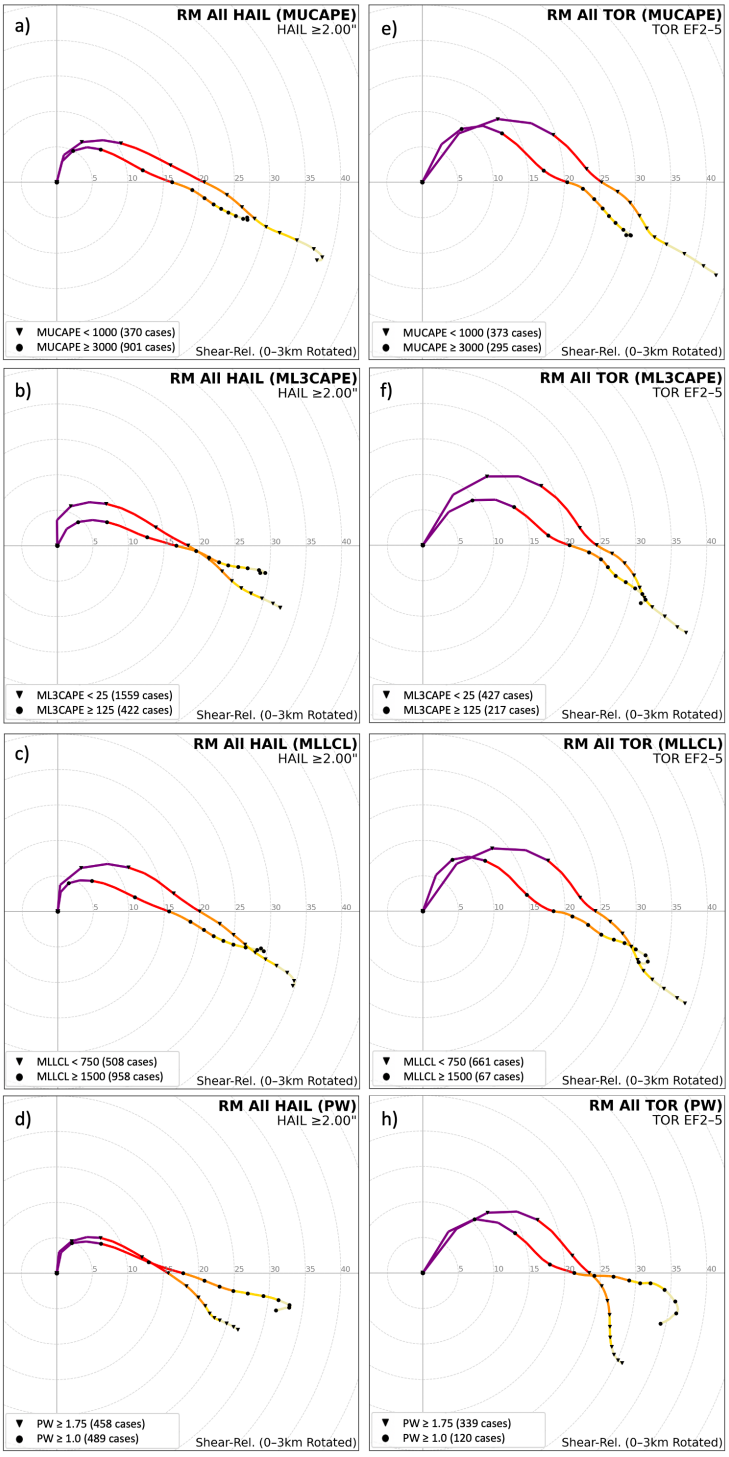

FIG. 10. Composite shear-relative hodograph comparisons for RM significant hail-producing supercells as a conditional function of (a) MUCAPE, (b) ML3CAPE, (c) MLLCL, and (d) PW, and for RM significant tornado-producing supercells as a conditional function of (e) MUCAPE, (f) ML3CAPE, (g) MLLCL, and (h) PW. The two hodographs displayed represent both the cases below the lower threshold and above the upper threshold for each of the variables used. The colored lines are the mean composite hodographs for each sample (purple is 0–1 km, red is 1–3 km, orange is 3–6 km, yellow is 6–9 km, and light yellow is 9–12 km). Winds are in m s^{-1}.

Accepted for publication in *Weather and Forecasting*. DOI 10.1175/WAF-D-21-0136.1.

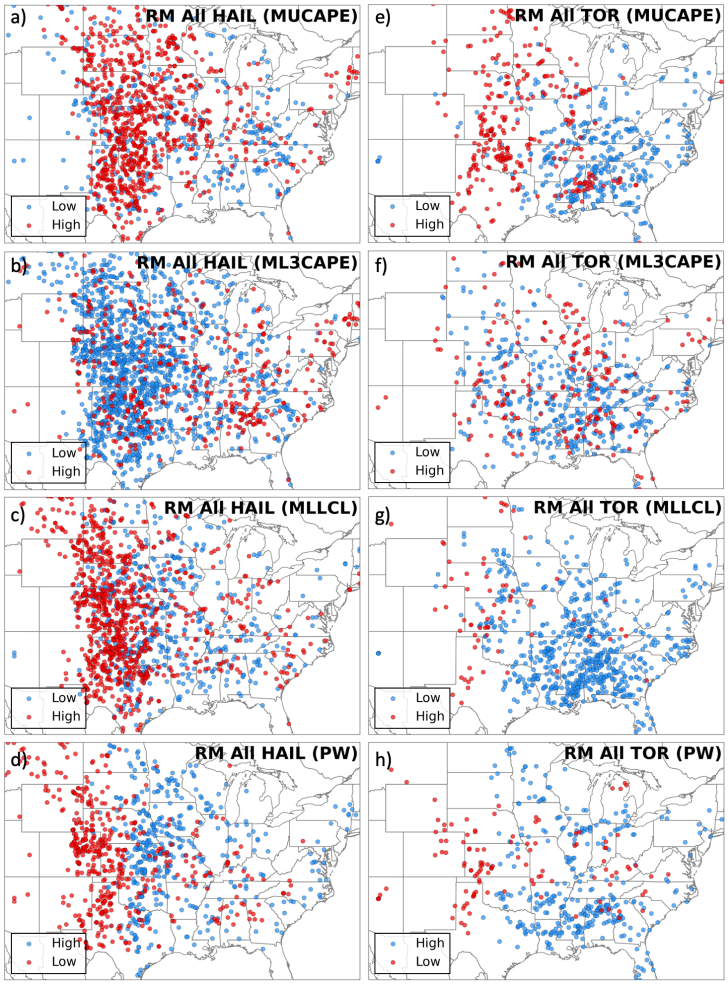

FIG. 11. Maps of locations for cases in each sample. The dots represent the locations of each report, and are colored based on which thermodynamic constraint was used. The thresholds for "Low" and "High" for each variable can be found in Fig. 10.

Accepted for publication in *Weather and Forecasting.* DOI 10.1175/WAF-D-21-0136.1.

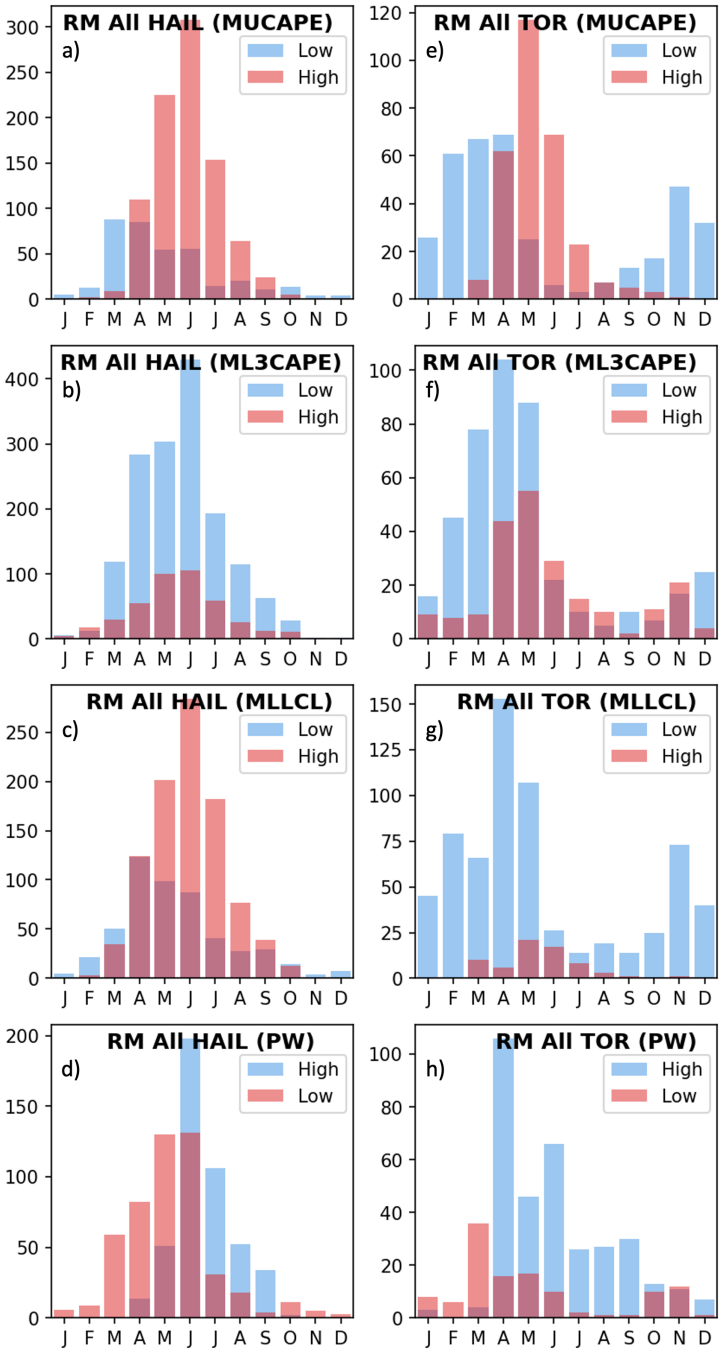

FIG. 12. Bar plot of cases in each month for each sample. The bars (and y-axis labels) represent the number of cases found in each month, and are colored based on which thermodynamic constraint was used. The thresholds for "Low" and "High" for each variable can be found in Fig. 10.

Accepted for publication in *Weather and Forecasting*. DOI 10.1175/WAF-D-21-0136.1.

For significant-severe hail cases (Fig. 10 a–d), low-level shear was weak across all samples, but pronounced differences could still be found in the low- and mid-level shear for different thermodynamic environments. The low-CAPE sample featured stronger shear in both of these layers than the high-CAPE sample (Fig. 10a), a relationship that was also found in ML3CAPE (Fig. 10b). The low ML3CAPE sample featured more veering of the shear vector with height in the lowest 3 km, while the high ML3CAPE sample displayed a comparatively straight hodograph. MLLCL height (Fig. 10c) also displayed a relationship with deep-layer shear, as well as the most pronounced disparity in low-level shear of any sample, with low LCL environments featuring stronger 0–1-km BWD. As with tornadic cases, the high-PW sample displayed weak deep-layer shear compared to the rest of the sample, with the low-PW sample displaying comparatively stronger shear above 1 km (Fig. 10d). The marginally severe hail cases (not shown) followed the same patterns, but with generally weaker BWD above 1 km.

4. Discussion

Perhaps one of the most operationally useful results from this study is a simple rule of thumb to distinguish between hodographs favoring severe hail from hodographs favoring tornadoes with supercells. Hail hodographs, when compared to tornadic hodographs, feature much weaker low-level shear and storm-relative helicity, and a resulting lower ratio of BWD below 1 km to BWD above 1 km. While tornado rating depends strongly on low-level shear, streamwise vorticity, and storm-relative inflow (a conclusion also supported by Nowotarski and Jones 2018; Coffer et al. 2020), it appears that hail size is only marginally predictable using the hodograph alone, especially toward larger sizes. However, it does appear that a certain hodograph shape is necessary for the production of severe hail. Such a hodograph features weak low-level shear and a weak meridional component of shear relative to the deep-layer shear (as supported by Johnson and Sugden 2014; Dennis and Kumjian 2017; Kumjian et al. 2019; Gutierrez and Kumjian 2021). It is currently unclear whether the weak meridional component or the weak low-level shear is most important for the hail process. However, these results strongly suggest that although hail-producing and tornadic cases feature similarly strong deep-layer shear, hail hodographs possess significantly weaker low-level shear than is associated with tornadoes. Such a pattern is a simple but powerful supplement to currently used forecast parameters and is easy to implement in the forecast process.

Accepted for publication in *Weather and Forecasting.* DOI 10.1175/WAF-D-21-0136.1.

We acknowledge a number of potential sources of error or bias in the dataset used for this study, though we also demonstrate that these have a negligible influence on the results. We also acknowledge a number of human error sources in hail reporting that cannot be tested herein, particularly that in instances of ongoing tornadoes, hail may be less likely to be reported due to its typically lesser potential threat to life and property. It is possible that this is a confounding factor in the disparity of low-level shear between hail-producing and tornadic cases. However, due to a lack of published literature, this is only speculation. Furthermore, our results and conclusions only support those of recent studies that demonstrate the importance of weak low-level shear in hail production both via simulations (e.g. Dennis and Kumjian 2017; Kumjian et al. 2021) and via observations with different datasets (e.g. Johnson and Sugden 2014; Kumjian et al. 2019; Gutierrez and Kumjian 2021). Therefore, regardless of potential biases, there is still strong evidence that the hodographs of hail-producing supercells and tornadic supercells are necessarily different.

The greatest skill in distinguishing hodographs of significant-severe hail from those of significant tornadoes came from considering low-level shear and streamwise vorticity. While 0–500-m SRH was on average greater than 175 m^2s^{-2} for significant tornadoes, it was generally less than 175 m^2s^{-2} for significant-severe hail. Though 0–1-km BWD tended to be greater than ~15 m s^{-1} for significant tornadoes, it was typically less than ~15 m s^{-1} for significant-severe hail. The 0–500-m and 0–1-km BWD were quite skillful at discriminating between significant hail and tornado environments with HSS over 0.45. The ratio of the low-level shear to the cloud-layer shear also showed considerable skill (HSS 0.42); the ratio of 0–1-km BWD to 1–6-km BWD was typically greater than ~0.75 for significant tornadoes, but less than ~0.75 for significant-severe hail. While it appears from the data that both strong shear above 1 km and weak shear below 1 km are associated with hail production, future work will be required to determine whether or not both of these conditions are actually necessary on a case-by-case basis, or if the ratio of this shear actually matters.

In contrast to tornadic hodographs, hodographs for severe hail-producing right-moving supercells had much weaker low-level BWD, streamwise vorticity, near-surface storm-relative wind, and storm-relative veering, with nearly all of the shear relatively straight and found above 1 km. This corroborates findings by Johnson and Sugden (2014), Dennis and Kumjian (2017), Kumjian and Lombardo (2020), and Kumjian et al. (2021). Upper-level winds were generally directed to the left of storm motion. Also in contrast to tornadic hodographs, hail-producing hodographs appeared

Accepted for publication in *Weather and Forecasting.* DOI 10.1175/WAF-D-21-0136.1.

to vary little between hail sizes, with only subtle increases in low-level shear and near-surface storm-relative winds. This is a key finding, as it suggests that differentiating between maximum hail sizes appears very difficult, if not impossible, with the shear profile alone. However, this does not mean that hail size is not predictable, nor that assessing thermodynamics alongside hodographs would not offer additional skill. Furthermore, the shapes of hodographs of various sizes closely resembled those found in smaller samples by Kumjian et al. (2019) and Gutierrez and Kumjian (2021). Of particular interest to severe hail forecasting, deep-layer BWDs such as the 0–6-km BWD, a parameter used in SHIP, showed very poor skill in size prediction, though this may be related to the exclusively supercell-based dataset used here. It must still be considered that a measure of deep-layer BWD may help to differentiate between convective modes, and that supercells account for the majority of severe hail production (Smith et al. 2012; Blair et al. 2017). No parameter showed a clear indication of appreciable forecast skill for significant-severe hail.

Though both RM and LM supercells in the United States can produce significant-severe hail, the means by which they do so, dependent on their internal storm structure, may be different. This hypothesis was drawn from the observation that their storm-relative wind profiles were dissimilar, especially in the direction of mid- and upper-level storm-relative winds relative to storm motion. How these environmental differences impact hail growth, and which storm-scale processes are most important for hail production in RM versus LM supercells, are potentially fruitful areas of future study.

In contrast to hail hodographs, hodographs of tornadic supercells featured much stronger low-level shear, streamwise vorticity, near-surface storm-relative wind, and storm-relative veering, with a large proportion of shear below 1 km. This is rather unsurprising and corroborates the leading theory that tornadoes are maintained and strengthened by the tilting and stretching of streamwise vorticity into a robust low-level mesocyclone. The best two discriminators between weak and strong tornadoes were SRH in the 0–500-m and 0–1-km layers, consistent with Coffer et al. (2019). The 0–3-km BWD, surface storm-relative wind, and 0–500-m SRH all displayed weak predictability in differentiating between strong and violent tornadoes. A backing of the shear vector above 2km was introduced as tornado strength increased, particularly for violent tornadoes. As stated prior, this is consistent with other composite hodographs in the literature, but may be an artifact of the smaller sizes of stronger tornadoes. Regardless, forecast discussions of severe

Accepted for publication in *Weather and Forecasting.* DOI 10.1175/WAF-D-21-0136.1.

convective weather still occasionally cite "veer-back" wind profiles as detrimental for supercell or tornado maintenance. We assert that much of these attributions are unfounded, especially since Parker (2017) also suggests that certain instances of backing aloft may have little effect on supercell maintenance, or even rather enhance it. Of particular interest to tornado forecasting, and consistent with Coffer et al. (2019), critical angle displayed poor performance, and in fact the *opposite* relationship to what is used in practice while forecasting significant tornadoes. This is likely a result of both its originally small testing sample and a compromised ability to estimate low-level $\widetilde{\omega_s}$.

The impact of the chosen thermodynamic variables on the mean hodograph shapes for each hazard and its magnitude revealed a few simple relationships, but with potentially complex origins and implications. That tornadic hodographs in low-CAPE environments featured much stronger low-level shear than those in high-CAPE environments was unsurprising given past literature (Guyer and Dean 2010; Sherburn and Parker 2014), since stronger low-level dynamic pressure perturbations assist tornado production. Of note, the mean hodograph for significant tornadoes in low-CAPE environments resembled the mean for all violent tornadoes, while the mean hodograph for significant tornadoes in high-CAPE environments resembled the mean for all weak tornadoes. There was a definite bias towards the Southeast U.S. and the winter and early spring months for low-CAPE environments, and toward the central/eastern longitudes of the Great Plains and the late spring and early summer months for high-CAPE environments. This suggests that location, time of year, and synoptic environment played a substantial role in modulating hodograph shape. However, this does not undermine the inverse relationship between CAPE and shear in severe weather environments that has been noted in past literature (e.g. Davies and Johns (1993) and Craven et al. (2004)). That ML3CAPE and MLLCL height have similar relationships with the hodograph is also not surprising, since low-level buoyancy can drive low-level updraft accelerations that support tornadoes (Davies 2002, 2006). The distinct relationship that PW displayed with tornadic hodograph shape was particularly intriguing. Like CAPE, the low- and high-PW samples were distinctly separated by region, where high PW cases were found mainly near the Gulf and Atlantic coasts as well as the Midwest corn belt, while low PW cases appeared confined to the central and southern high Plains. These samples were also somewhat distinct in time, with low-PW cases peaking earliest, and high-PW cases featuring a long tail into late summer. While

Accepted for publication in *Weather and Forecasting.* DOI 10.1175/WAF-D-21-0136.1.

enough literature exists to support the low-CAPE, high-shear relationship being of importance to tornadoes, little exists to support an analogous relationship between shear and moisture content. Therefore, future work is necessary to determine whether the resulting hodographs are simply a function of regional/seasonal difference, or if certain hodograph structures are actually necessary to complement or counteract the effects of high moisture content and precipitation loading in tornado production.

Though comparatively less work has been done to establish known relationships between thermodynamics and shear for large hail, the impact of the thermodynamic variables on supercells that produced large hail were also noticeable. A similar CAPE-shear relationship was evident, where shear both below and especially above 1 km was stronger when CAPE was lower, to produce any given hail size. This may suggest that stronger low-level storm-relative flow (which influences updraft width and associated dilution via entrainment per Peters et al. (2019, 2020)) may be necessary to sustain the updrafts of hail-producing supercells, especially in environments with weak buoyancy. As with tornadoes, a decrease in low-level CAPE and LCL height was associated with larger hodographs. This may suggest that low-level updraft accelerations play a similar role in hail production, but this may also simply be function of these thermodynamic profiles occuring most often in synoptic environments characterized by strong baroclinicity. The association of higher PW with weaker shear above 1 km resembled that of the tornadic cases, with a noticeable eastward shift over the Plains as PW increased; the relationship between moisture content and shear profile in hail production would also benefit from future examination.

5. Concluding Remarks

We examined hodographs from a large sample of severe hail and tornado reports to understand the potential influence of the shear profile on the type and magnitude of potential severe weather. Potential hail size above the severe threshold was not found to show obvious predictability using the hodograph alone, unlike tornado rating. However, the hodograph shape associated with severe hail production was found to be quite different from that associated with tornadoes. Though a number of biases in hail reporting may influence these results, those that were testable demonstrated negligible influence. These results also support the conclusions of a growing number of both observational and modeling studies on the structure of hailstorms as governed by the shear profile.

Accepted for publication in *Weather and Forecasting.* DOI 10.1175/WAF-D-21-0136.1.

We proposed a simple rule of thumb to differentiate between hodographs of severe hail-producing vs. tornadic supercells. Weaker shear in the lowest kilometer, especially where shear above 1 km is proportionately much stronger, serves as a distinguishing characteristic of hodographs associated with severe hail-producing supercells. These results are relevant not only to the operational forecasting of hazards, but also the numerical modeling of supercells, where it is critical to understand what base shear profile is necessary to produce the desired storm structure. For instance, if future studies similar to Kumjian et al. (2021) chose to simulate hailstorms using a traditional tornadic hodograph, they may not achieve the desired results. Future work will supplement the shear profile with thermodynamics, so that simulations of supercells can employ even more realistic environments for hail growth. Certain approximations of the thermodynamic profile, namely deep-layer buoyancy and precipitable water, appeared to strongly influence the shear profile that was necessary to produce a given hazard. Most unmistakably, to compensate for low buoyancy, stronger shear especially below 1 km was necessary in tornadic cases, while stronger shear especially above 1 km was necessary in hail-producing cases. However, regardless of the thermodynamic profile, hodograph shape appears to be a simple and effective way to distinguish between the environments of severe hail and tornadoes.

Accepted for publication in *Weather and Forecasting.* DOI 10.1175/WAF-D-21-0136.1.

Acknowledgments. This research was based upon work supported by the National Science Foundation under Grant No. AGS-1855054. This research was also supported by the Earth and Ecosystem Science PhD program at Central Michigan University. We would like to acknowledge Alex Schueth of Texas Tech University for inspiring a detailed analysis of low-level storm-relative inflow parameters. We would also like to acknowledge Matthew Wilson of the University of Nebraska–Lincoln for contributing code that was used in this study.

Data availability statement. The filtered dataset of all reports of hail ≥1.00" and tornadoes EF0–EF5 along with an extensive list of proximal environmental parameters originally included by Smith et al. (2012) and Thompson et al. (2012), as well as a corresponding vertical profile of RAP state variables for each report, is available upon request.

APPENDIX A

Potential impacts of data collection inconsistencies on results

a. Duplicate cases

A total of 762 soundings used in this analysis were found to be duplicates, such were included in the composites of both hail-producing and tornadic supercells. Due to concerns that this would significantly affect our results, we produced plots of the hodographs of severe hail-producing (Fig. *A*1) and tornado-producing (Fig. *A*2) supercells. Despite the large number of duplicate cases, this did not appear to make a noticeable difference in the mean shear profiles examined herein, thus do not appear to influence the results and conclusions.

b. Sampling differences

As noted by Warren et al. (2021), reports of hail under 2” were only collected for the purposes of this dataset for the years 2014–2015. Furthermore, during this time, the criteria for data collection was inconsistent. Due to concerns that this would significantly impact the smallest size bin of our study (1.00–1.75”), we produced plots of hodographs for all hail sizes in only the years 2014–2015, and compared these with those formed from the larger sample size used in this study (Fig. *A*3). Fortunately, the sample of all hail cases from 2014–2015 displayed very similar

Accepted for publication in *Weather and Forecasting.* DOI 10.1175/WAF-D-21-0136.1.

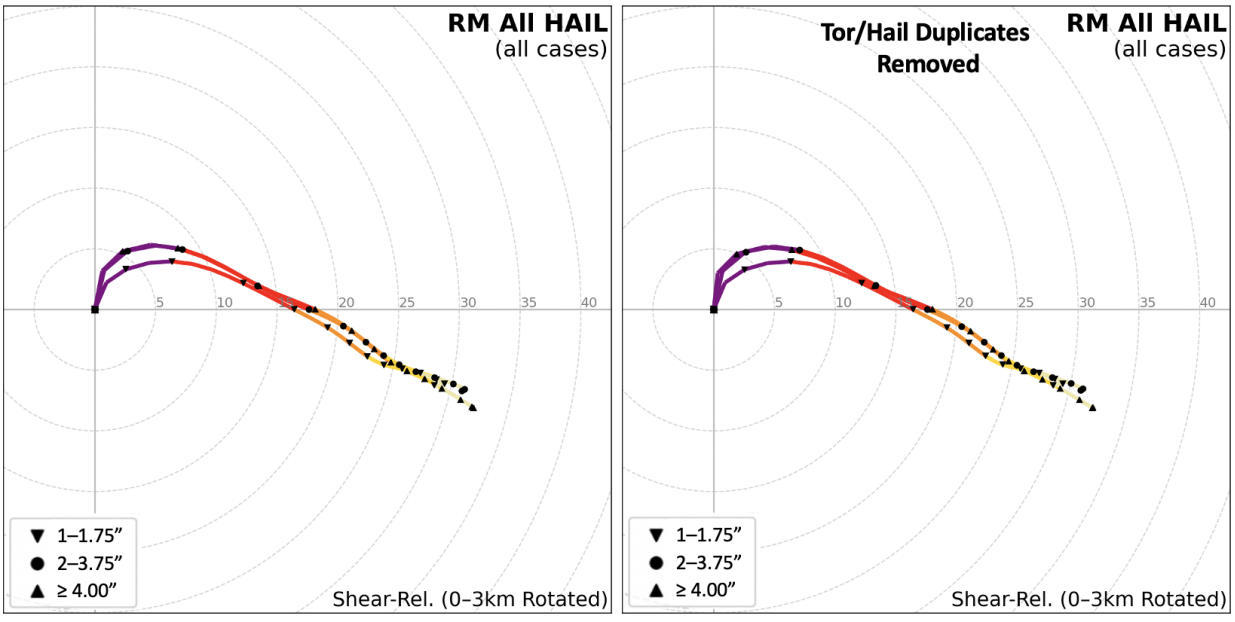

FIG. A1. Composite shear-relative hodographs for (left) all discrete severe hail-producing RM supercells (with the hodograph for hail 1.00–1.75" marked by downward-pointing triangles, 2.00–3.75" marked by circles, and greater than or equal to 4.00" marked by upward-pointing triangles), and (right) all of these cases but with tornado/hail duplicates removed. The colored line is the mean composite hodograph (purple is 0–1 km, red is 1–3 km, orange is 3–6 km, yellow is 6–9 km, and light yellow is 9–12 km). Winds are in m s^{-1}.

hodograph characteristics to the full sample, thus these inconsistencies and limited climatology do not appear to have significantly influenced the results of this paper.

Accepted for publication in *Weather and Forecasting.* DOI 10.1175/WAF-D-21-0136.1.

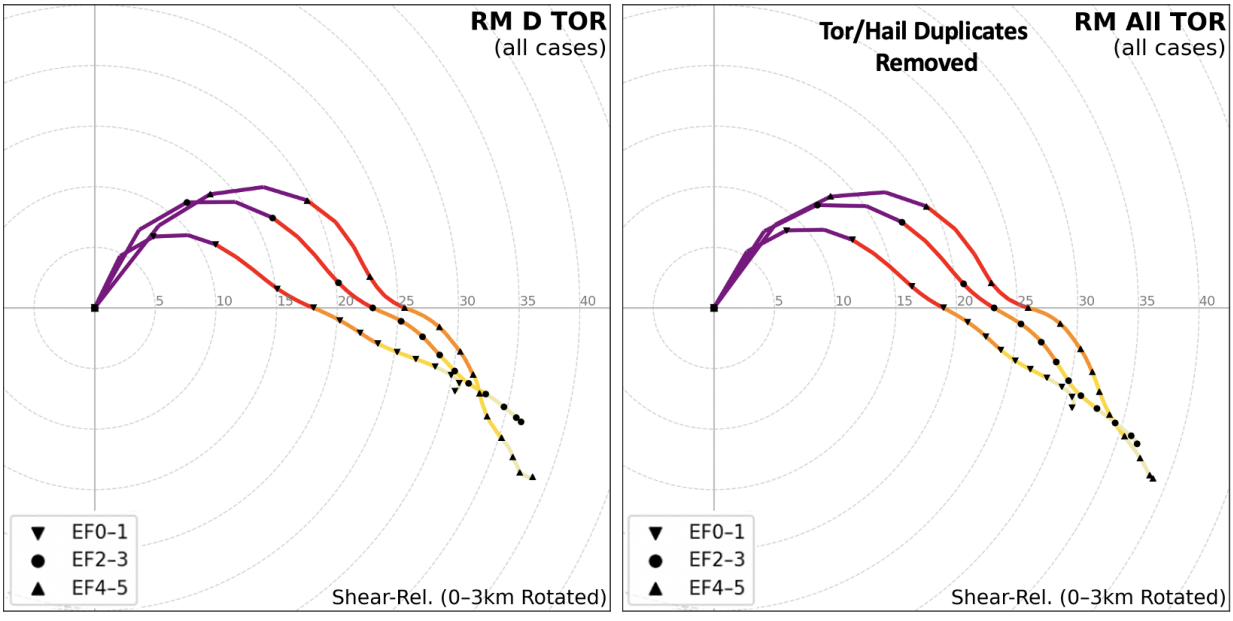

FIG. A2. Composite shear-relative hodographs for (left) all discrete severe tornado-producing supercells (with the hodograph for EF0–1 tornadoes marked by downward-pointing triangles, EF2–3 marked by circles, and EF4 or stronger marked by upward-pointing triangles), and (right) all of these cases but with tornado/hail duplicates removed. The colored line is the mean composite hodograph (purple is 0–1 km, red is 1–3 km, orange is 3–6 km, yellow is 6–9 km, and light yellow is 9–12 km). Winds are in m s^{-1}.

Accepted for publication in *Weather and Forecasting.* DOI 10.1175/WAF-D-21-0136.1.

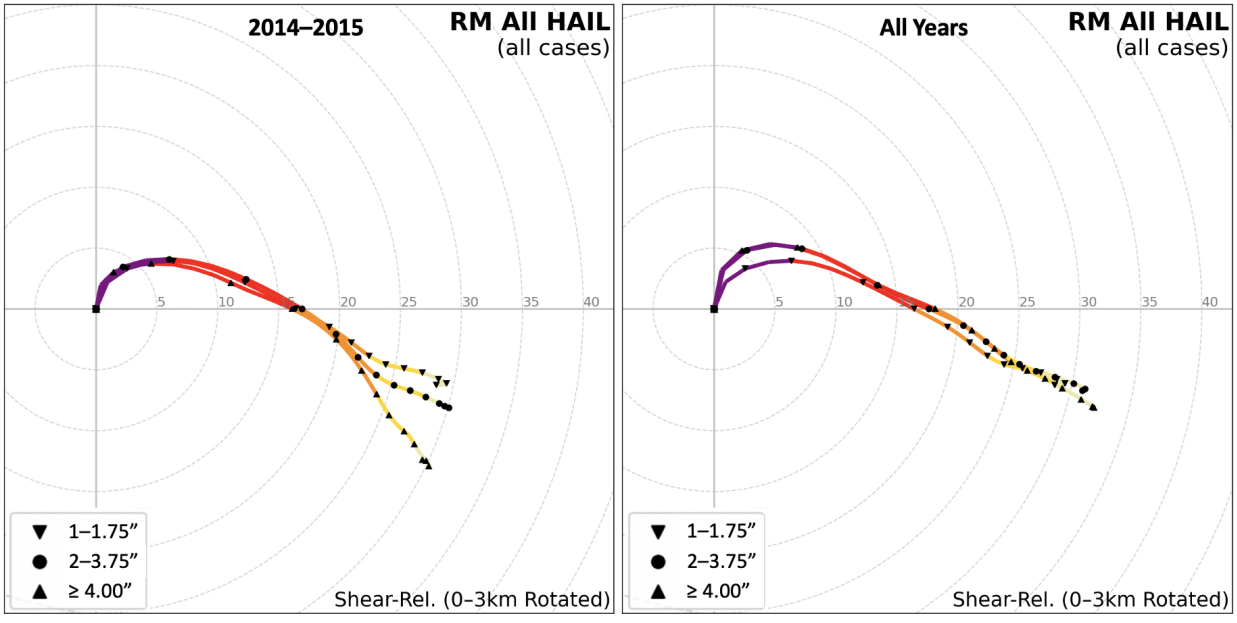

FIG. A3. Composite shear-relative hodographs for (right) all discrete severe hail-producing RM supercells (with the hodograph for hail 1.00–1.75" marked by downward-pointing triangles, 2.00–3.75" marked by circles, and greater than or equal to 4.00" marked by upward-pointing triangles), and (left) only cases from 2014–2015. The colored line is the mean composite hodograph (purple is 0–1 km, red is 1–3 km, orange is 3–6 km, yellow is 6–9 km, and light yellow is 9–12 km). Winds are in m s^{-1}.

Accepted for publication in *Weather and Forecasting.* DOI 10.1175/WAF-D-21-0136.1.

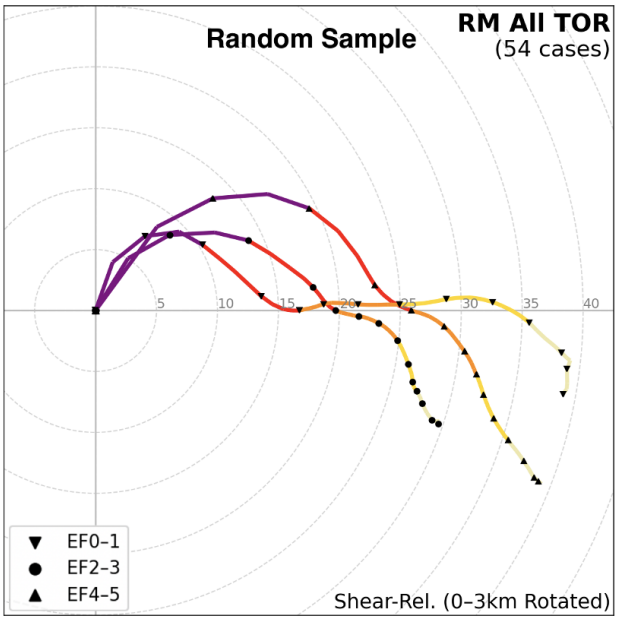

FIG. A4. Composite shear-relative hodographs for all discrete severe tornado-producing supercells (with the hodograph for EF0–1 tornadoes marked by downward-pointing triangles, EF2–3 marked by circles, and EF4 or stronger marked by upward-pointing triangles). The colored line is the mean composite hodograph (purple is 0–1 km, red is 1–3 km, orange is 3–6 km, yellow is 6–9 km, and light yellow is 9–12 km). Winds are in m s^{-1}.

c. Underrepresentation of violent tornado cases

The sample of violent tornadoes examined in this study was small, at only 54. Care was taken not to make firm conclusions based on insubstantial inferences from this sample. That said, the backing of the shear vector aloft for the violent tornado sample was an intriguing finding, and it was necessary to test whether or not this added structure in the hodograph was simply a result of having less cases to make up the composite. To address this, we produced a plot of hodographs made up of a random sample of cases of each rating, each with the same number of cases as the violent tornado sample. This exercise reveals that a similar backing structure also appears in the hodographs of the weak and strong tornado samples, so it follows that the backing aloft in the violent tornado sample may also be due to its small sample size. Thus, we do not conclude that backing aloft is more prevalent in violent tornadoes.

Accepted for publication in *Weather and Forecasting.* DOI 10.1175/WAF-D-21-0136.1.

References

Allen, J. T., and M. K. Tippett, 2015: The characteristics of United States hail reports: 1955-2014. *Electron. J. Severe Storms Meteorol.*, **10**, 1–31.

Allen, J. T., M. K. Tippett, Y. Kaheil, A. H. Sobel, C. Lepore, S. Nong, and A. Muehlbauer, 2017: An extreme value model for US hail size. *Mon. Wea. Rev.*, **145**, 4501–4519.

Ashley, W. S., 2007: Spatial and temporal analysis of tornado fatalities in the United States: 1880–2005. *Wea. Forecasting*, **22**, 1214–1228.

Baumgardt, D., 2011: Hail estimation: How good are your spotters? NOAA, http://www.crh.noaa.gov/arx/hail_size_MSP.pdf.

Blair, S. F., and Coauthors, 2017: High-resolution hail observations: Implications for NWS warning operations. *Wea. Forecasting*, **32**, 1101–1119.

Bothwell, P. D., B. T. Smith, R. L. Thompson, A. R. Dean, and J. S. Kain, 2014: Severe weather parameter reanalysis project at the Storm Prediction Center. *Preprints, 27th Conf. on Severe Local Storms, Madison, WI, Amer. Meteor. Soc.*

Brooks, H. E., J. W. Lee, and J. P. Craven, 2003: The spatial distribution of severe thunderstorm and tornado environments from global reanalysis data. *Atmos. Res.*, **67-68**, 73–94.

Brown, R. A., 1993: A compositing approach for preserving significant features in atmospheric profiles. *Mon. Wea. Rev.*, **121**, 874–880.

Bunkers, M. J., 2002: Vertical wind shear associated with left-moving supercells. *Wea. Forecasting*, **17**, 845–855.

Bunkers, M. J., J. S. Johnson, L. J. Czepyha, J. M. Grzywacz, B. A. Klimowski, and M. R. Hjelmfelt, 2006: An observational examination of long-lived supercells. Part II: Environmental conditions and forecasting. *Wea. Forecasting*, **21**, 689–714.

Bunkers, M. J., B. A. Klimowski, J. W. Zeitler, R. L. Thompson, and M. L. Weisman, 2000: Predicting supercell motion using a new hodograph technique. *Wea. Forecasting*, **15**, 61–79.

Coffer, B. E., and M. D. Parker, 2017: Simulated supercells in nontornadic and tornadic VORTEX2 environments. *Mon. Wea. Rev.*, **145**, 149–180.

Accepted for publication in *Weather and Forecasting.* DOI 10.1175/WAF-D-21-0136.1.

Coffer, B. E., M. D. Parker, R. L. Thompson, B. T. Smith, and R. E. Jewell, 2019: Using near-ground storm relative helicity in supercell tornado forecasting. *Wea. Forecasting*, **34**, 1417–1435.

Coffer, B. E., M. Taszarek, and M. D. Parker, 2020: Near-ground wind profiles of tornadic and nontornadic environments in the United States and Europe from ERA5 reanalyses. *Wea. Forecasting*, **35**, 2621–2638.

Concannon, P. R., H. E. Brooks, and C. A. Doswell, 2000: Climatological risk of strong and violent tornadoes in the United States. *Preprints, 2nd Symp. on Environmental Applications, Long Beach, CA, Amer. Meteor. Soc*, 212–219.

Coniglio, M. C., 2012: Verification of RUC 0–1-h forecasts and SPC mesoscale analyses using VORTEX2 soundings. *Wea. Forecasting*, **27**, 667–683.

Coniglio, M. C., and R. E. Jewell, 2021: Spc mesoscale analysis compared to field-project soundings: Implications for supercell environment studies. *Mon. Wea. Rev.*

Coniglio, M. C., and M. D. Parker, 2020: Insights into supercells and their environments from three decades of targeted radiosonde observations. *Mon. Wea. Rev.*, **148**, 4893–4915.

Craven, J. P., H. E. Brooks, J. A. Hart, and Coauthors, 2004: Baseline climatology of sounding derived parameters associated with deep, moist convection. *Natl. Wea. Dig*, **28**, 13–24.

Davies, J. M., 2002: Significant tornadoes in environments with relatively weak shear. *Preprints, 21st Conf. on Severe Local Storms, San Antonio, TX, Amer. Meteor. Soc*, Vol. 16.

Davies, J. M., 2006: Tornadoes in environments with small helicity and/or high LCL heights. *Wea. Forecasting*, **21**, 579–594.

Davies, J. M., and R. H. Johns, 1993: Some wind and instability parameters associated with strong and violent tornadoes: 1. Wind shear and helicity. *Geophys. Monogr. Ser.*, **79**, 573–582.

Davies-Jones, R., 1990: Test of helicity as a forecast parameter. *Preprints, 16th Conf. on Severe Local Storms, Kananaskis Park, AB, Canada, Amer. Meteor. Soc.*, 588–592.

Dennis, E. J., and M. R. Kumjian, 2017: The impact of vertical wind shear on hail growth in simulated supercells. *J. Atmos. Sci.*, **74**, 641–663.

Accepted for publication in *Weather and Forecasting.* DOI 10.1175/WAF-D-21-0136.1.

Doswell, C. A., R. Davies-Jones, and D. L. Keller, 1990: On summary measures of skill in rare event forecasting based on contingency tables. *Wea. Forecasting*, **5**, 576–585.

Esterheld, J. M., and D. J. Giuliano, 2008: Discriminating between tornadic and non-tornadic supercells: A new hodograph technique. *Electron. J. Severe Storms Meteor.*, **3**, 1–50.

Galway, J. G., 1975: Relationship of tornado deaths to severe weather watch areas. *Mon. Wea. Rev.*, **103**, 737–741.

Gunturi, P., and M. Tippett, 2017: Impact of ENSO on US tornado and hail frequencies. Managing Severe Thunderstorm Risk, Technical Report. *Willis Re*.

Gutierrez, R. E., and M. R. Kumjian, 2021: Environmental and radar characteristics of gargantuan hail-producing storms. *Mon. Wea. Rev.*, **149**, 2523–2538.

Guyer, J. L., and A. R. Dean, 2010: Tornadoes within weak CAPE environments across the continental United States. *Preprints, 25th Conf. on Severe Local Storms, Denver, CO, Amer. Meteor. Soc. A*.

Hitchens, N. M., and H. E. Brooks, 2012: Evaluation of the Storm Prediction Center's day 1 convective outlooks. *Wea. Forecasting*, **27**, 1580–1585.

Hyvärinen, O., 2014: A probabilistic derivation of Heidke skill score. *Wea. Forecasting*, **29**, 177–181.

Jewell, R., and J. Brimelow, 2009: Evaluation of Alberta hail growth model using severe hail proximity soundings from the United States. *Wea. Forecasting*, **24**, 1592–1609.

Johns, R. H., J. M. Davies, and P. W. Leftwich, 1993: Some wind and instability parameters associated with strong and violent tornadoes. 2. Variations in the combinations of wind and instability parameters. *Geophys. Monogr. Ser.*, **79**, 583–583.

Johnson, A. W., and K. E. Sugden, 2014: Evaluation of sounding-derived thermodynamic and wind-related parameters associated with large hail events. *Electron. J. Severe Storms Meteor.*, **9**.

Knight, C. A., and N. C. Knight, 2001: Hailstorms. Severe Convective Storms. *Meteorological Monographs*, **28**, 223–254.

Accepted for publication in *Weather and Forecasting.* DOI 10.1175/WAF-D-21-0136.1.

Kumjian, M. R., Z. J. Lebo, and A. M. Ward, 2019: Storms producing large accumulations of small hail. *J. Appl. Meteorol. Climatol*, **58**, 341–364.

Kumjian, M. R., and K. Lombardo, 2020: A hail growth trajectory model for exploring the environmental controls on hail size: Model physics and idealized tests. *J. Atmos. Sci.*, **77**, 2765–2791.

Kumjian, M. R., K. Lombardo, and S. Loeffler, 2021: The evolution of hail production in simulated supercell storms. *J. Atmos. Sci. (In Press)*, https://doi.org/10.1175/JAS-D-21-0034.1.

Lemon, L. R., and C. A. Doswell, 1979: Severe thunderstorm evolution and mesocyclone structure as related to tornadogenesis. *Mon. Wea. Rev.*, **107**, 1184–1197.

Maddox, R. A., 1976: An evaluation of tornado proximity wind and stability data. *Mon. Wea. Rev.*, **104**, 133–142.

Markowski, P., C. Hannon, J. Frame, E. Lancaster, A. Pietrycha, R. Edwards, and R. L. Thompson, 2003: Characteristics of vertical wind profiles near supercells obtained from the Rapid Update Cycle. *Wea. Forecasting*, **18**, 1262–1272.

May, R. M., S. C. Arms, P. Marsh, E. Bruning, J. R. Leeman, K. Goebbert, J. E. Thielen, and Z. S. Bruick, 2021: Metpy: A Python package for meteorological data. Unidata, url-https://github.com/Unidata/MetPy, https://doi.org/10.5065/D6WW7G29.

Nowotarski, C. J., and A. A. Jensen, 2013: Classifying proximity soundings with self-organizing maps toward improving supercell and tornado forecasting. *Wea. Forecasting*, **28**, 783–801.

Nowotarski, C. J., and E. A. Jones, 2018: Multivariate self-organizing map approach to classifying supercell tornado environments using near-storm, low-level wind and thermodynamic profiles. *Wea. Forecasting*, **33**, 661–670.

Parker, M. D., 2014: Composite VORTEX2 supercell environments from near-storm soundings. *Mon. Wea. Rev.*, **142**, 508–529.

Parker, M. D., 2017: How much does "backing aloft" actually impact a supercell? *Wea. Forecasting*, **32**, 1937–1957.

Accepted for publication in *Weather and Forecasting.* DOI 10.1175/WAF-D-21-0136.1.

Peters, J. M., C. J. Nowotarski, and H. Morrison, 2019: The role of vertical wind shear in modulating maximum supercell updraft velocities. *J. Atmos. Sci.*, **76**, 3169–3189.

Peters, J. M., C. J. Nowotarski, J. P. Mulholland, and R. L. Thompson, 2020: The influences of effective inflow layer streamwise vorticity and storm-relative flow on supercell updraft properties. *J. Atmos. Sci.*, **77 (9)**, 3033–3057.

Potvin, C. K., K. L. Elmore, and S. J. Weiss, 2010: Assessing the impacts of proximity sounding criteria on the climatology of significant tornado environments. *Wea. Forecasting*, **25**, 921–930.

Rasmussen, E. N., and J. M. Straka, 1998: Variations in supercell morphology. Part I: Observations of the role of upper-level storm-relative flow. *Mon. Wea. Rev.*, **126**, 2406–2421.

Rotunno, R., J. B. Klemp, and M. L. Weisman, 1988: A theory for strong, long-lived squall lines. *J. Atmos. Sci.*, **45**, 463–485.

Schaefer, J. T., and J. Galway, 1981: Population biases in the tornado climatology. *Bull. Amer. Meteor. Soc.*, Vol. 62, 1402–1402.

Schaefer, J. T., J. J. Levit, S. J. Weiss, and D. W. McCarthy, 2004: The frequency of large hail over the contiguous united states. *Preprints, 14th Conf. on Applied Climatology, Seattle, WA, Amer. Meteor. Soc*, Citeseer, Vol. 3.

Schneider, R. S., A. Dean, S. Weiss, and P. Bothwell, 2006: Analysis of estimated environments for 2004 and 2005 severe convective storm reports. *Preprints, 23rd Conf. Severe Local Storms, St. Louis MO, Amer. Meteor. Soc., 6pp., CD-ROM*, Vol. 3.

Sherburn, K. D., and M. D. Parker, 2014: Climatology and ingredients of significant severe convection in high-shear, low-CAPE environments. *Wea. Forecasting*, **29**, 854–877, https://doi.org/10.1175/WAF-D-13-00041.1.

Smith, B. T., R. L. Thompson, J. S. Grams, C. Broyles, and H. E. Brooks, 2012: Convective modes for significant severe thunderstorms in the contiguous United States. Part I: Storm classification and climatology. *Wea. Forecasting*, **27**, 1114–1135, https://doi.org/10.1175/WAF-D-11-00115.1.

Accepted for publication in *Weather and Forecasting.* DOI 10.1175/WAF-D-21-0136.1.

Taszarek, M., J. T. Allen, T. Púčik, K. A. Hoogewind, and H. E. Brooks, 2020: Severe convective storms across Europe and the United States. Part II: ERA5 environments associated with lightning, large hail, severe wind, and tornadoes. *J. Clim.*, **33**, 10 263–10 286.

Thompson, R. L., and R. Edwards, 2000: An overview of environmental conditions and forecast implications of the 3 May 1999 tornado outbreak. *Wea. Forecasting*, **15**, 682–699.

Thompson, R. L., R. Edwards, and J. A. Hart, 2002: Evaluation and interpretation of the supercell composite and Significant Tornado Parameters at the Storm Prediction Center. *Preprints, 21st Conf. on Severe Local Storms, San Antonio, TX, Amer. Meteor. Soc*, Citeseer.

Thompson, R. L., R. Edwards, J. A. Hart, K. L. Elmore, and P. Markowski, 2003: Close proximity soundings within supercell environments obtained from the Rapid Update Cycle. *Wea. Forecasting*, **18**, 1243–1261, https://doi.org/10.1175/1520-0434(2003)018<1243:CPSWSE>2.0.CO;2.

Thompson, R. L., R. Edwards, and C. M. Mead, 2004: An update to the supercell composite and significant tornado parameters. *Preprints, 22nd Conf. on Severe Local Storms, Hyannis, MA, Amer. Meteor. Soc. P*, Vol. 8.

Thompson, R. L., C. M. Mead, and R. Edwards, 2007: Effective storm-relative helicity and bulk shear in supercell thunderstorm environments. *Wea. Forecasting*, **22**, 102–115.

Thompson, R. L., B. T. Smith, J. S. Grams, A. R. Dean, and C. Broyles, 2012: Convective modes for significant severe thunderstorms in the contiguous United States. Part II: Supercell and QLCS tornado environments. *Wea. Forecasting*, **27**, 1136–1154.

Wade, A. R., M. C. Coniglio, and C. L. Ziegler, 2018: Comparison of near-and far-field supercell inflow environments using radiosonde observations. *Mon. Wea. Rev.*, **146**, 2403–2415.

Warren, R. A., H. Richter, and R. L. Thompson, 2021: Spectrum of near-storm environments for significant severe right-moving supercells in the contiguous United States. *Mon. Wea. Rev.*, **149**, 3299–3323.

Weisman, M. L., and J. B. Klemp, 1986: Characteristics of isolated convective storms. *Mesoscale meteorology and forecasting*, Springer, 331–358.

Accepted for publication in *Weather and Forecasting.* DOI 10.1175/WAF-D-21-0136.1.